Giant Radio Array for Neutrino Detection (GRAND)

Measurements of the Analog Antenna and
the Relation between the Shape of the Signal and the
Depth of the Shower

Jikke Tacken
s4691555

Bachelor Thesis Physics

Supervisor: Charles Timmermans
Radboud University
High Energy Physics
July 2020

Abstract

The Giant Radio Array for Neutrino Detection (GRAND) is building their second prototype GP300 of 300 antennas. These can detect the electromagnetic signal of the showers created by cosmic rays and neutrinos at low elevation angles. The analog part of the antennas (the low noise amplifier, normal amplifier and filter) is measured for the whole chain and the three separate parts with a vector network analyser (VNA). The measurements of the separate parts are combined together and compared with the measurements of the whole chain. Both have a (almost) constant amplification in the region GRAND uses for measurements ($50-200$MHz). The cutoff frequencies of the amplification are around 25 and 230 MHz and the decrease in amplification is very steep at these location. The delay of the measurements changes 25 ns in the frequency range, most of it between 50 and 100 MHz. The x polarisation of the antenna is shifted with respect to the y and z polarisation. The measurements of the separate parts are different from the measurements of the whole chain. Why these two last facts happened is not clear. The second part of this work looks at one of the properties of the signal that will be measured: the full width of the peak at half maximum (FWHM). Signals of five cosmic rays are modelled with five different depths (X_{max}) for the showers. The FWHM values are compared and there was a significant difference in FWHM values for different values of X_{max}. A difference in X_{max} values of 142 g/cm^2 has a difference in FWHM of $3-4\sigma$ and for smaller ΔX_{max} of $25-45$ g/cm^2 the difference in FWHM is still 1σ (depending on which fit was used to describe the peak). Further research has to show if this difference in FWHM remains after the data have been corrected for the antenna.

Contents

Introduction . . . 3

1 Theory **4**
1.1 Cosmic Rays . . . 4
1.1.1 The Particle Shower . . . 4
1.1.2 The Electromagnetic Signal . . . 6
1.2 GRAND . . . 11
1.2.1 The Antenna . . . 13

2 Measurements of the Analog Part of the Antenna **16**
2.1 Method . . . 16
2.2 Results . . . 20
2.2.1 Amplitude Gain . . . 20
2.2.2 Phase Shift and Time Delay . . . 22
2.3 Conclusion . . . 23

3 Analysis of the Cosmic Ray induced Air Shower Signal **27**
3.1 Method . . . 27
3.2 Results . . . 32
3.3 Conclusion . . . 39

Appendix A Antenna Measurements from China **42**

Appendix B Extra Figures Antenna Measurements **44**

Appendix C Plots of FWHM vs ψ vs θ **47**

Appendix D Plots of FWHM vs θ with the Fits of all Five Depths **50**

Introduction

Little is still knows about the origin of cosmic rays with higher energies. For energies of 10^{17} eV and higher the origin is outside the Milky Way. What process produce these particles is (yet) unknown. The cosmic rays create neutrinos and gamma rays in their interaction with the cosmic microwave background. Measuring these high energy cosmic rays and neutrinos gives more information about their origin and properties. The Giant Radio Array for Neutrino Detection (GRAND) will be built to measure these particles. Its antennas can detect the electromagnetic signal of the showers created by cosmic rays and neutrinos at low elevation angles. Therefore a lot of antennas have to be build. The first prototype GP35, with 35 antennas, is already build and the second GP300, with 300 antennas, is underway. The goal of this second prototype is to show the feasibility of the measurements. Since the amount of antennas is still to small to measure neutrinos, this will be tested with cosmic rays only.

This research paper consists of two parts. The first contains the measurements of the properties of the antennas for GP300. The analog part of the antenna is measured to see how it changes the signal. The amplification of the amplitude and the delay of the signal are measured. This tells us how much the original signal changes and if it is possible to reconstruct the data from the signal that went through the antenna. In the second part we look at one of shower properties that are stored in the original data, the depth of the cosmic ray shower (X_{max}). The signal that the shower of a cosmic ray produces has a peak at the beginning and a small dip afterwards. The full width of this peak at half its maximum (FWHM) is connected to the depth of the shower. The signal of five different shower depths is created with the ZHAires air shower simulation package. This produces the signal of the shower at a number of antenna location. The FWHM values of the peaks are calculated and the relation with the depth of the shower (X_{max}) investigated.

1 Theory

GRAND stands for Giant Radio Array for Neutrino Detection, a collection of radio antennas for measuring cosmic rays and neutrinos with energies of 10^{17} eV or higher. This paper only looks at the cosmic rays. In the theory section, I will first look at how a cosmic ray produces a particle shower and how that produces an electromagnetic signal. Secondly, I will discuss how this signal can be measured by GRAND.

1.1 Cosmic Rays

Cosmic rays are charged particles. These particles are nuclei stripped from all their electrons during their journey through space. Most are protons (90%) and alpha particles (9%) and the last 1% is comprised of heavier nuclei.[1] The majority of cosmic rays with energies below 10^{17} eV are from inside our galaxy and cosmic rays with higher energies are probably from outside the Milky Way. Around $10^{19.6}$ eV a cutoff in the flux of cosmic rays is measured. Why there are no cosmic rays measured beyond this point is not (yet) clear.[2] GRAND measures primary particles with energies of 10^{17} eV and up, so mostly of extragalactic origin.

1.1.1 The Particle Shower

When a cosmic ray enters the atmosphere it interacts with molecules in the atmosphere and produces secondary particles. The situation is simplest if the primary particle is a proton[i], this kind of shower is shown in figure 1.1 left. When a proton interacts with an air molecule it produces mostly pions. Around $2/3$ of the pions are charged pions $\pi^{\pm}$ and the other $1/3$ are neutral pions π^0. The π^0 decays immediately into photons (γ) and the $\pi^{\pm}$ interact again and create more π^0 and other

[i] It is the same for a neutron, but these are not stable unless bound in a nucleus.

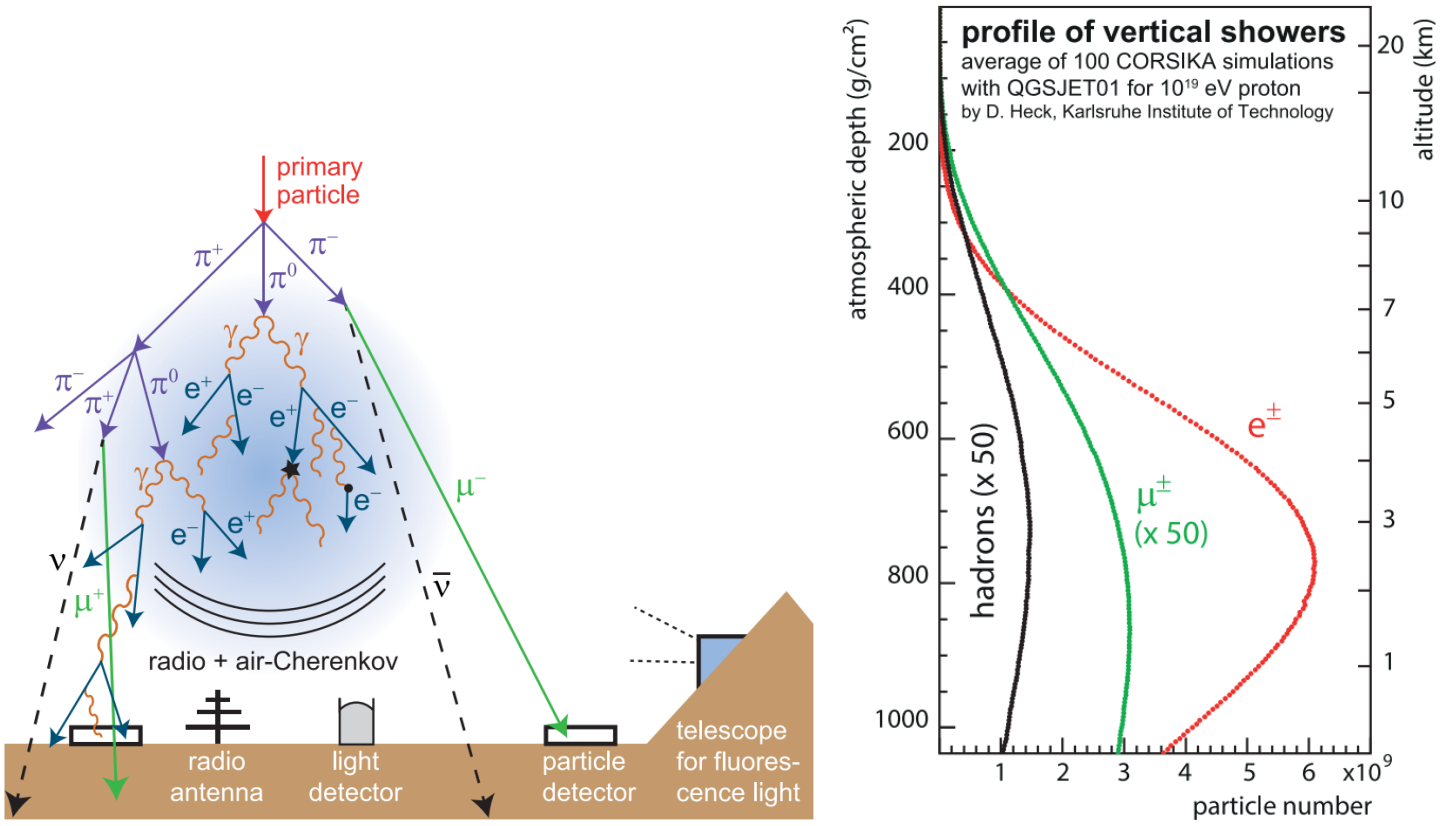

Figure 1.1: The left figure gives an general idea of the particle shower of a cosmic ray (not all decays and interactions are correct). The right figure shows how many particles exist during the development of the shower.[2]

particles. The photons create an electron e^- and positron e^+ via pair production, or ionise atmospheric atoms to free more electrons that become part of the shower (the Compton effect). The electrons from ionisation produce a negatively charged shower front. The excess of e^- can be as large as $20-30\%$ of the total number of $e^\pm$. The created $e^\pm$, in turn, create more photons, electrons and positrons through bremsstrahlung and the inverse Compton effect. This way the amount of $e^\pm$ increases until the particle energies fall below the critical energy. Below this energy the particles decay before they interact again and have too little energy for bremsstrahlung or the inverse Compton effect.[2,3,4] The air shower can have a lateral distance of several kilometres, but the electron density quickly decreases with lateral distance.[2]

When the primary particle is not a single photon or neutron, but an alpha particle or heavier nucleus with A protons and/or neutrons the superposition model tells us that it can be approximated by A proton showers, all with $1/A$ of the total energy of the primary particle.[3]

The height at which the shower consists of most particles is called X_{max}. This maximum is expressed in atmospheric depth (g/cm^2), the air mass that the particle traversed. The right side of figure 1.1 shows the development of the amount of particles in a shower. X_{max} is important because it can tell something about the primary particle. The maximum is shallower for heavier particles compared to protons with the same energy. First, because the size of the nucleus is roughly proportional to the number of protons and neutrons, thus a heavier element interacts higher in the atmosphere (lower X_{max}).[2] Second, because the shower of a heavier particle can be approximated with A proton showers, each with $1/A$ of the energy of the cosmic ray.[4] All A showers have a smaller start energy, thus reach the critical energy earlier. The difference between the X_{max} of a proton and an iron particle is around 100 g/cm^2 for the showers that GRAND measures.[5]

1.1.2 The Electromagnetic Signal

Production of the Emission

The electrons and positrons in the showerfront create an electromagnetic signal. The signal is mainly produced by two phenomena: geomagnetic deflection and the Askaryan effect.

The geomagnetic deflection is the main effect causing the radio emission for air showers, see figure 1.2 left. The Earth's magnetic field creates a Lorentz force on the moving charged particles.

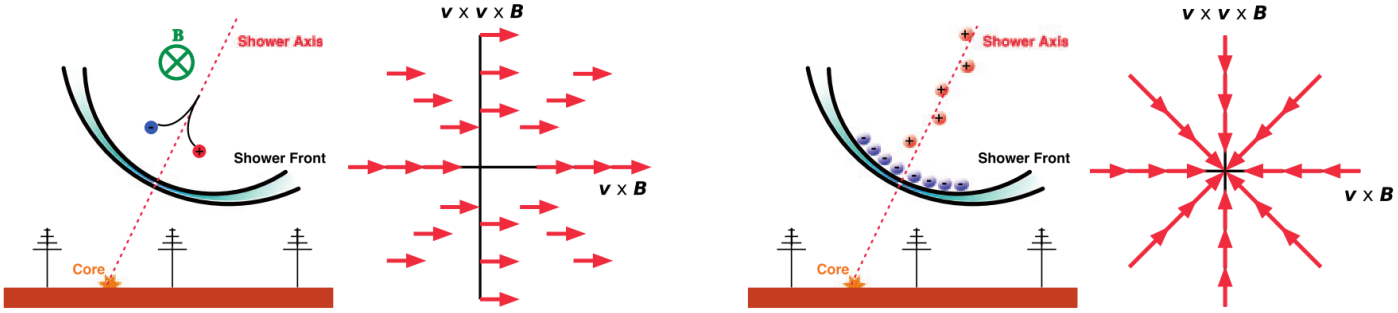

Figure 1.2: Left the geomagnetic effect and right the Askaryan effect. Both vector fields are seen from below the showerfront looking up. The travel direction of the shower ($\hat{v}$) is out of the paper and the magnetic field ($\vec{B}$) is down. The Earth magnetic field is from south to north, thus $\vec{v} \times \vec{B}$ is west.[6]

$$\mathbf{F}_{Lorentz} = q(\mathbf{E} + \mathbf{v} \times \mathbf{B})$$

Only the electrons and positrons play a significant role in creating this geomagnetic emission. Both travel in opposite directions perpendicular to the magnetic field and the shower axis. This force accelerates the electrons and positrons. How much the electrons and positrons are accelerated depends on the angle between the shower direction and the magnetic field and the strength of the field. This in turn determines the amplitude of the emission. The constant interactions with atmospheric particles decreases the acceleration, creating an almost constant drift velocity, similar to electrons in a wire. This way the particles form a transverse current perpendicular to the air-shower axis and Earth magnetic field. The magnitude of the current changes during the evolution of the air shower. First it grows until the shower reaches its maximum amount of $e^{\pm}$ at X_{max} after which it decreases again. The flux in the electric field creates an electromagnetic wave with a linear polarisation parallel to the current.[6,2]

The Askaryan effect contributes about 10% of the electric field amplitude or 1% of the level of radiated power to the electromagnetic signal. This effect is created as result of the ionisation of atmospheric particles via the Compton effect. The ionisation makes the showerfront negatively charged and leaves behind a trace of positively charged atoms and molecules around the shower axis. The showerfront can therefore be viewed as a negative point charge that changes in strength during the shower evolution. The electromagnetic waves are polarised

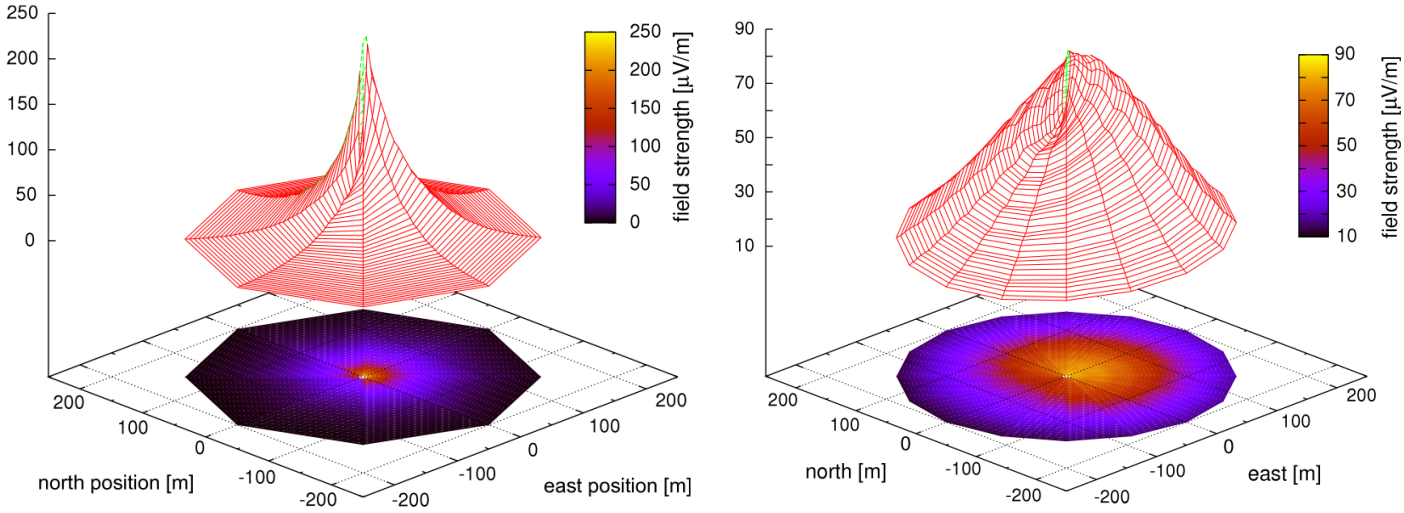

(a) Footprint of a proton.

(b) Footprint of an iron nucleus.

Figure 1.3: The footprints of two vertical showers with different primary particles with energies of 10^{17} eV at the LOPES site.[7]

radially and its magnitude is zero at the shower axis, because the changing electric field is like that of a point charge, see the right side of figure 1.2. That means that the polarisation as seen by an observer, or antenna, depends on their location relative to the shower core.[6,2]

Shape of the Emission

The particles in front of the shower travel with almost the speed of light in vacuum and the electromagnetic waves travel with the speed of light in air. This shapes the waves into a narrow forward beam with a duration that is compressed to between zero and a few hundred nanoseconds. The duration of the pulse depends on the distance from the shower core. At the Cherenkov angle this effect creates a cone at which the signals from large parts of the shower arrive at (almost) the same time. Here the pulse is the shortest. The pulse becomes longer the further away from Cherenkov angle the observer is. For showers with a zenith angle of 60 degrees (the kind used in this paper) the Cherenkov angle is just above 1 degree.[8]

The power of the total emission depends on the amount of electrons in the shower. The number of electrons is approximately proportional to the energy of the primary particle and the emission scales quadratically with the amount of

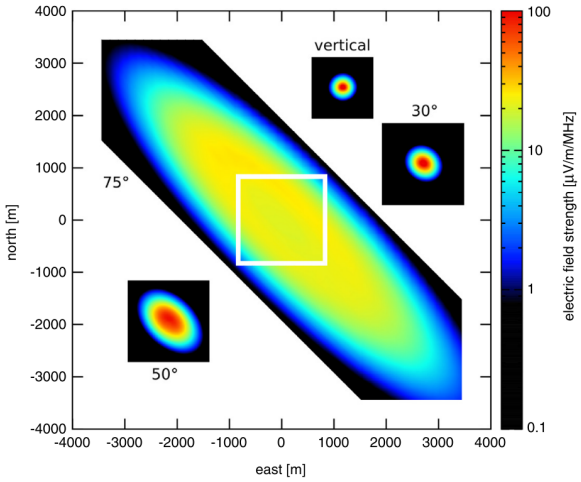

Figure 1.4: The simulated footprints of the radio emission of a shower in the 30–80 MHz frequency band with different zenith angles. The shower has an energy of 5×10^{18} eV. The shower footprint becomes larger for larger zenith angles. The white square is the size of the 50° footprint.[7]

electrons. This means that the power of the emission scales quadratically with the energy of the primary particle. Most of the radiation is created around X_{max} and within one meter of the shower axis. The showerfront has a thickness of around 1 meter, which makes the emission coherent and strongly amplified for wavelengths of 1 meter or more.[2]

The total signal of the shower is the addition of signals of the geomagnetic deflection and the Askaryan effect that reaches Earth. The polarisation from the geomagnetic deflection is everywhere in the direction of the Lorentz force and the polarisation of the Askaryan effect is radial, thus depends on the azimuth angle between the shower and the observer. Since the observation of the Askaryan effect depends on the location of the observer relative to the shower core, this is also true for the total signal. If the polarisation directions of the Askaryan and geomagnetic mechanisms are in the same direction the signal increases and if they are opposite the signal decreases as is visible in figure 1.3 for the signal of a proton and iron nucleus. The field strength is significantly stronger to the east of the shower core, because there both polarisations are in the same direction.

The footprint of the shower also depends on distance (in meters) of X_{max} from the observer. For particles that follow the same path that distance from the ground to the maximum of the shower is larger if the primary particle is heavier. For

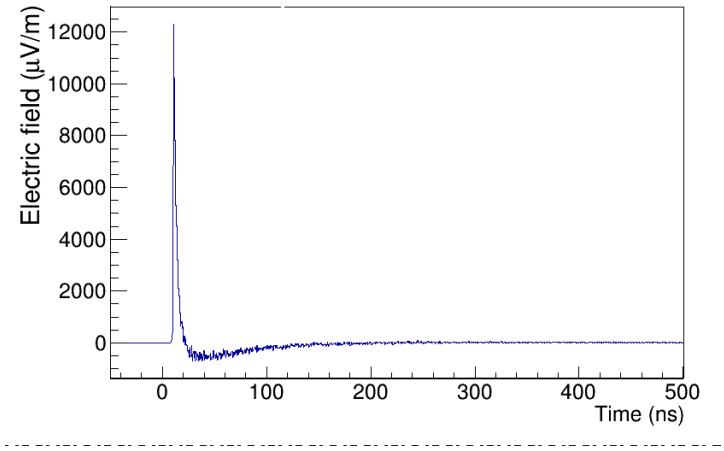

(a) The signal at angle $\theta = 2.25$, close to the Cherenkov angle and the shower core.

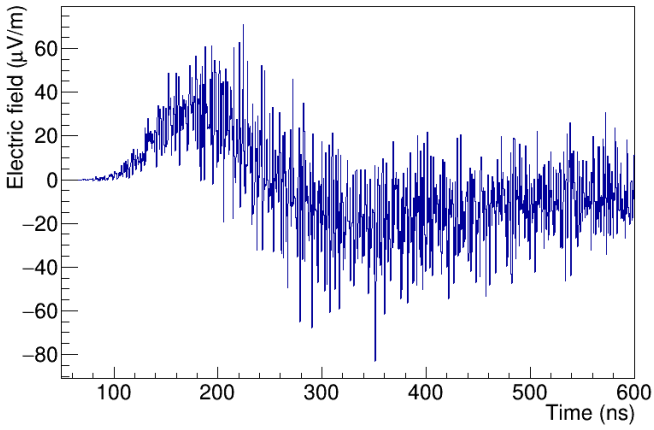

(b) The signal at angle $\theta = 12.44$, far away from the Cherenkov angle and the shower core.

Figure 1.5: The two graphs are from the modelled showers used in this paper. Both are from a shower with $X_{max} = 756.97$ g/m^2 and at $\psi = -90$. For the definitions of θ and ψ see figure 3.1. The pulse represents the signal that is received by the y-direction of an antenna of GRAND.

those particles X_{max} is smaller, which means that the shower maximum is earlier and thus higher in the atmosphere. The difference is visible in figure 1.3. This distance is even more influenced by the angle between the vertical and the shower axis, the zenith angle. A larger angle means a longer path in the atmosphere and thus a larger footprint. Figure 1.4 shows the footprints for different zenith angles. A larger footprint means that the radiated power is distributed over a larger area and thus the average electric field strength is lower.[7]

As said before the signal is a short pulse. It does not only vary with location, but also with time. The pulse has a high peak and then a dip below zero. The shape depends on the distance from the shower core, and the azimuth angle as described above. For this paper the width of the peak is the most important. Figures 1.5a and 1.5b show a modelled shower of the electric field used for this paper. 1.5a is near the core and 1.5b is further away. The signal clearly becomes longer and has a smaller amplitude further away from the shower core. The smaller amplitude means that the noise becomes more dominant in comparison to the signal, as is clearly visible.

1.2 GRAND

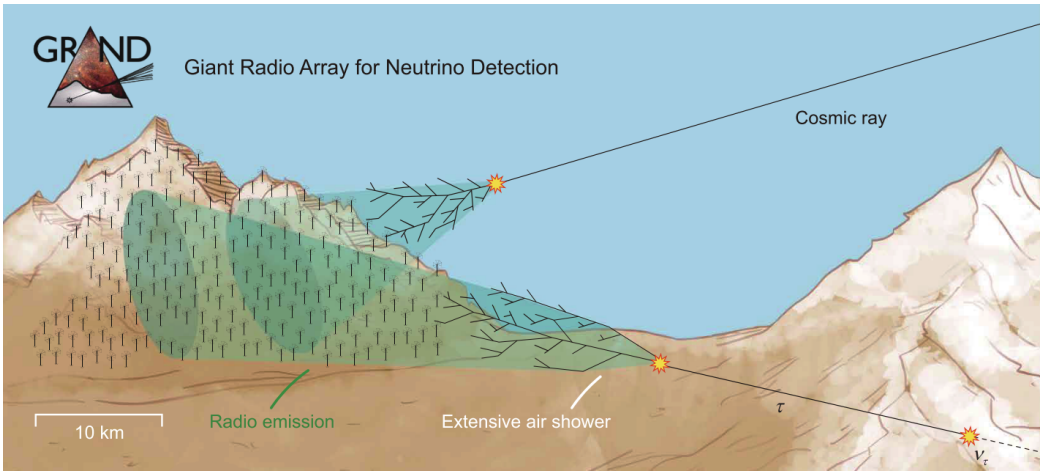

Figure 1.6: The GRAND detection principle with 10,000 antennas. The ultra high energy cosmic rays and gamma rays (not shown in the image) interact in the atmosphere and produce an air shower. The neutrinos interact underground and create an air shower via a high energy tau lepton. The air showers are measured by the antennas of GRAND.[5]

The Giant Radio Array for Neutrino Detection (GRAND) will be a collection of thousands of identical antennas spaced at a distance of 1 km. The plan is to have 200,000 antennas in the 2030s, divided into about 20 independent arrays of roughly 10,000 antennas each. The first prototype is already built and the installation of the second is now in progress. GRAND will be used to search for the origin of ultra high energy cosmic rays (UHECRs), which have energies of 10^{18} eV or higher.

UHECRs have been observed for more than fifty years, but little is yet known about them. They are probably created outside our galaxy and appear to be made in powerful cosmic accelerators, yet none have been identified. During their paths through space the cosmic rays change directions due to cosmic magnetic fields. Our incomplete knowledge of the properties of UHECRs and the effect of the magnetic fields on their path makes it impossible to trace them back to their source. For sources far away it is even more difficult since cosmic rays with energies above 4×10^{19} eV often do not reach the Earth from distances beyond 100 Mpc, due to their interactions with the cosmic microwave background (CMB).

Figure 1.7: GR300 mechanical construction on top of Xidian University. The antenna, the pole the triangular box and the sandbox are visible.[9]

This limits the statistics of UHECRs and their sources.

In the interactions between UHECRs and the CMB ultra-high-energy (UHE) gamma rays and neutrinos are also produced, which are unaffected by cosmic magnetic fields. In addition, these may be produced inside the source, so detecting them and their direction can point directly to the origin of the UHECRs. UHE gamma rays cannot reach Earth from beyond 10 Mpc as result of interactions with the CMB, but the UHE neutrinos are unaffected and can reach Earth from all distances. The antennas of GRAND will detect the showers of UHE neutrinos, gamma rays and cosmic rays. A gamma ray air shower is similar to that of a cosmic ray, but X_{max} is deeper. If a neutrino decays it also produces a shower and a radio pulse similar to that of a cosmic ray, but the chance of it interacting in the air is much smaller.

By focusing on showers with a large zenith angle the antennas of GRAND can be spaced much further apart (1 km) compared to the requirement for more vertical showers, since the footprint is much larger for these showers, see figure 1.3. This makes it affordable to cover a much larger area with antennas, and thus detect more showers. The location of GRAND is chosen such that almost horizontal showers travel through a mountain range close by. This blocks the cosmic ray and gamma ray showers from reaching the antennas from that direction, but increases

the chance for the neutrinos to interact. This makes it also possible to separate the neutrinos from the UHECRs and gamma rays, and, as described before, the UHECRs and gamma rays can be separated by their difference in X_{max}. GRAND will be sensitive for cosmic rays and gamma rays with zenith angles between 65° and 85°.

The first prototype of GRAND was the GRANDProto35 (GP35) built in 2018, consisting of 35 antennas. Now the second prototype is being tested: GRANDProto300 (GP300) with 300 antennas. The main goal of GP300 is to demonstrate the viability of the detection principle of GRAND. This means that it can trigger on nearly horizontal air showers, separate them from the background noise, and reconstruct their properties, such as the mass of the primary particle, with similar or better precision as techniques that are already used for cosmic ray detection. The GP300 array will not be large enough for neutrino detection, thus all these parts will be tested with UHECRs. This will of course provide a lot of data of UHECRs interesting for further analyses.[5]

1.2.1 The Antenna

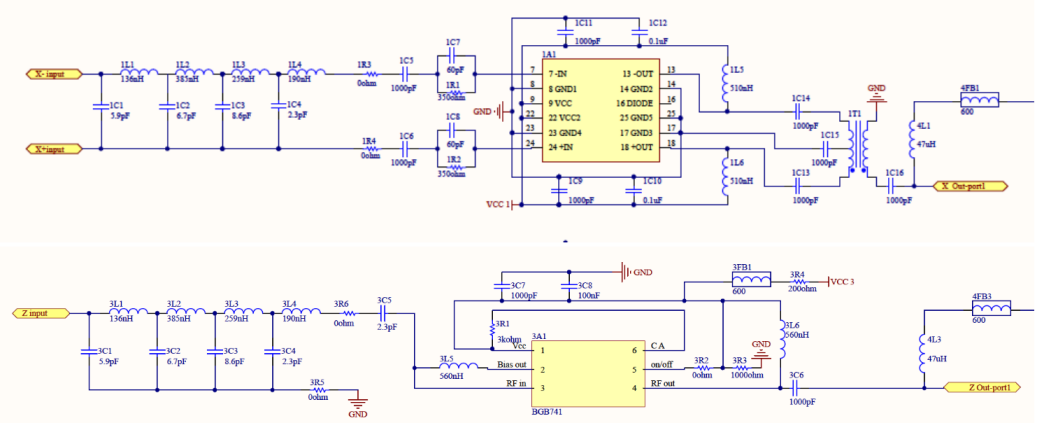

Figure 1.8: At the top the LNA circuit used for the x and y polarisation, and on the bottom the LNA circuit for the z polarisation.[9]

The antenna designed for GRAND is called the HorizonAntenna and is made to have a high detection efficiency along the horizon. A photo of what the antenna looks like, complete with pole and electronics box, is shown in figure 1.7. The antenna is comprised of five identical arms, that measure the North-South (x),

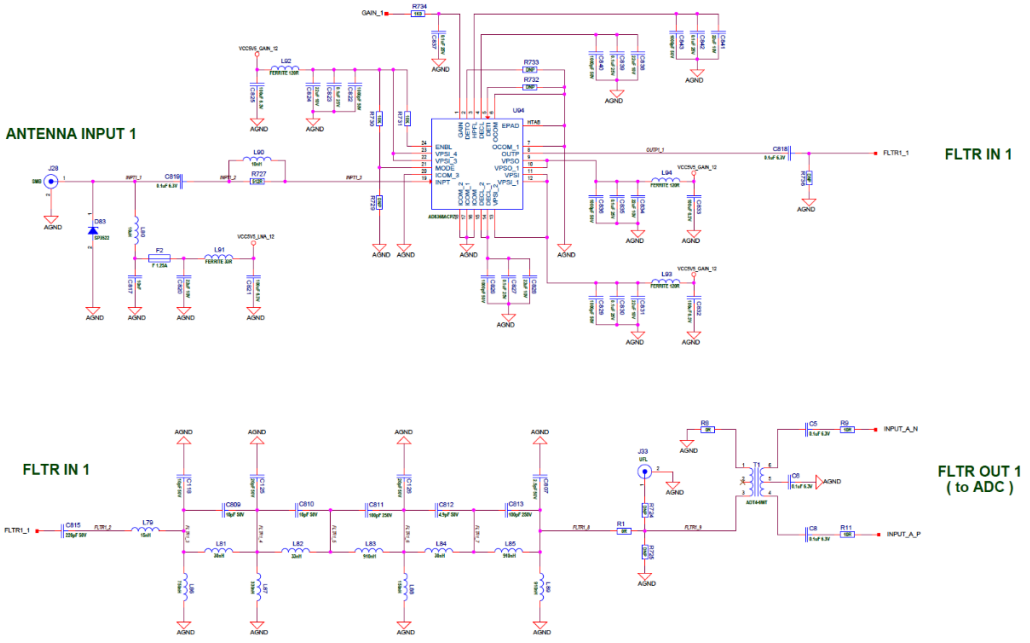

Figure 1.9: A schematic view of the analog part of the main board. The signal comes in from the LNA at the top part on the left. The signal is amplified (top) and then filtered (bottom) and leaves at the bottom right to be digitised.[9]

East-West (y) and vertical (z) polarisation separately. The arm to the North and to the South together form a dipole antenna, and the same for the arms to the East and West, and the upward arm forms a monopole antenna to measure the vertical direction.

At the top of the pole the x, y and z directions are connected to Low Noise Amplifiers (LNAs). The LNAs for the x and y direction are identical, but the LNA for the z direction has a different chip, see figure 1.8. The first part of the electronics chain is attached to the antenna and is used to match the impedance of the circuit to the antenna to ensure maximal transmission. This is very similar for all three channels. Next comes the LNA chip, for the x and y channel this is the Linear Technology LTC6430-20, with a gain of 20.9 dB and a noise figure of 2.9 dB in the $50 - 200$ MHz range. For the z channel the Infineon BGB741 is used. This one has a gain of 21 dB and a noise figure of 1.1 dB. The final part of the electronics chain is to match the impedance to the 50 Ω of the transmission cable.

After the LNAs amplify the signal it is sent through a 5 m long cable to the

rest of the electronics in the triangular box at the bottom of the pole. The power that the LNA chips use is received from the main board by the same cable via a bais-T. The power used by each LNA is 0.8 W at an input voltage level of 5.5 V.

The rest of the electronics are situated on the main board. The signal is AC coupled through a bias-T. The signal can be amplified by an AD8368 amplifier. This has a variable amplification to adjust the sensitivity of the antenna-system to the magnitude of the electric field. This improves the sensitivity for lower energy showers, and reduces the noise for higher energy showers since the noise added by this amplifier depends on the gain. The chip has a gain span of 34 dB, starting at -12 dB, a noise figure of 9.5 dB at maximum gain and consumes 440 mW.

The amplifier is followed by a elliptic $30-200$ MHz bandpass filter. It is a compromise between a sharp cutoff at the edges and a constant group delay as a function of frequency. The constant group delay is important, because a delay that changes with frequency changes the shape of the electric pulse. That means for the measured data the shape is distorted, which may not be completely recoverable. Measurements, such as the X_{max} of the shower, depend on an accurate knowledge of the signal shape. To keep the delay constant the phase shift has to increase linear with the frequency.[10] After going through the filter the data is digitised.[9] The digitisation and more details about the antenna are described in [9].

2 Measurements of the Analog Part of the Antenna

The analog part of the antenna is characterised to see how the signal changes before it is digitised. Knowing how the signal changes is necessary to gain accurate knowledge of the signal shape of the recorded air shower, and to use this to obtain knowledge of the properties of the primary particle. The change in amplitude and phase of the signal is investigated for the whole range of frequencies of the GRAND detector.

2.1 Method

The measurement is done in two parts: the whole analog chain is measured together, and all parts are measured separately. The measurements are preformed in cooperation with Dániel Szálas-Motesiczky. The analog chain consist of three parts: the low noise amplifier (LNA), the on board amplifier and the filter. The description of these parts and how they will be connected in the antenna is given in section 1.2.1. A vector network analyser[i] (VNA) was used to create the signal as well as to measure the result. Separate sources[ii] were used to supply the power for the chips in the LNA and the amplifier.

The VNA measures the scattering parameters (s-parameters) of the connected device. These parameters indicate how the signal is transmitted through and reflected by the device. Figure 2.1 shows the s-parameters for a device with two connections. The VNA produces a signal and sends it forward or reverse trough the device. Since the VNA sends the signal itself, it knows the incident signal and it can measure the reflected and transmitted signal. The VNA keeps track of

[i] The VNA was the ZNB4 from Rohde & Schwarz.

[ii] The power source was the HMC8043 power supply from Rohde & Schwarz

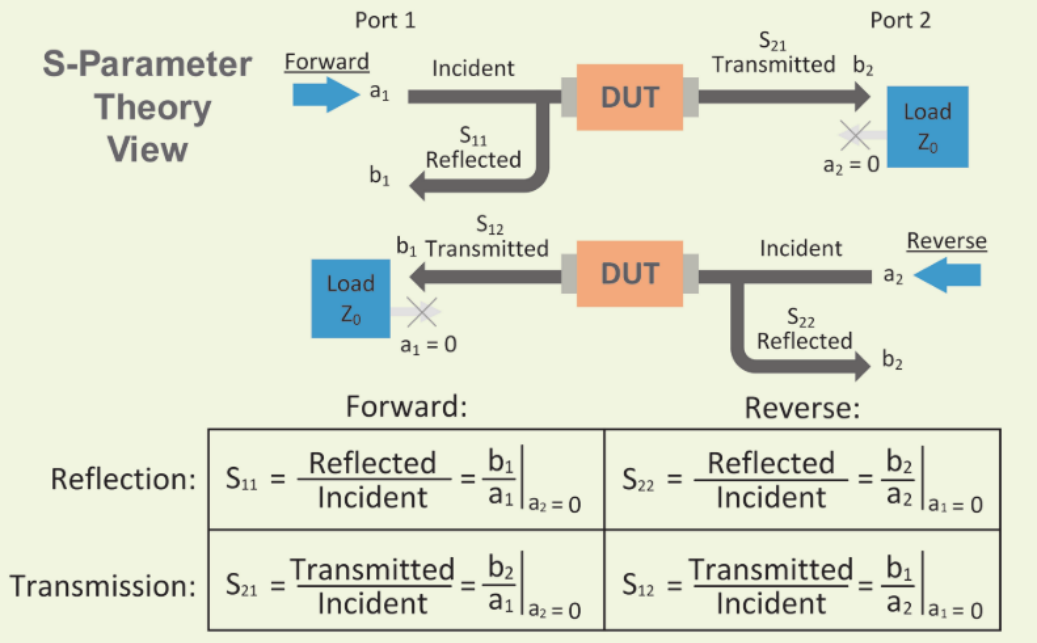

Figure 2.1: The s-parameters and how the VNA calculates them.[11]

both the amplitude and phase of all three signals. The phase changes are given in degrees and the amplitude changes in decibel. The most interesting s-parameter is S_{21}, because that indicates how the output signal of the antenna will look. The signal produced by the VNA was set to sweep over the frequency range $0-300$ MHz to know the phase and amplitude changes for all these frequencies. The range of frequencies measured by GRAND, $50-200$ MHz, falls well within this range.[11]

Decibels give the amplification of the amplitude compared to reference amplitude, in this case the amplitude of the input. It is calculated with:

$$\mathrm{dB} = 20\log\left(\frac{A_2}{A_1}\right) \tag{2.1}$$

Where A_1 is the amplitude of the input signal of the VNA and A_2 is the amplitude of the transmitted signal.

The separate amplifier and filter are measured by Dániel Szálas-Motesiczky using a single input and output of the VNA. The VNA was calibrated such that the influence of the connection wires was eliminated. For the amplifier the external power source was connected to set the gain. The voltage determines the gain.

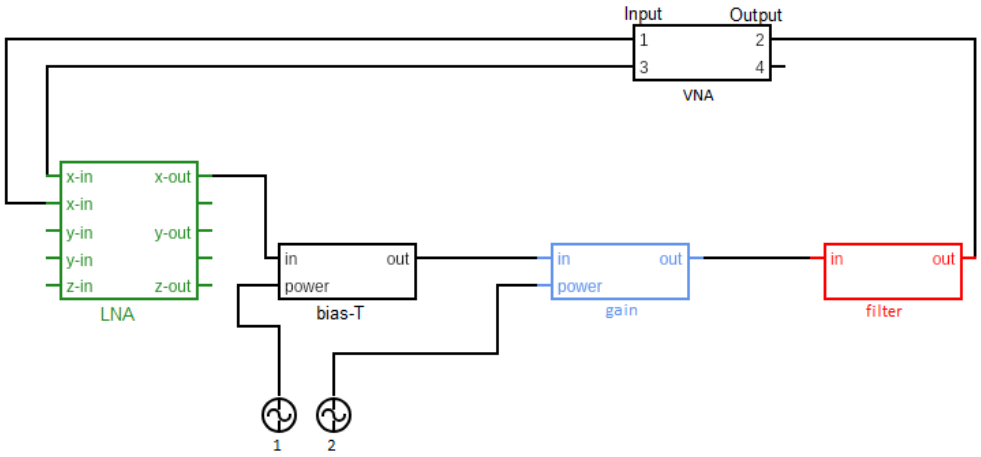

Figure 2.2: The schematic sketch of the complete analog chain connected to the VNA for measurements. Here the x polarisation is measured.

From 100 mV to 900 mV they are related by:

$$Gain = 37.5 \times V_{gain} - 14 \tag{2.2}$$

With gain in dB and voltage (V_{gain}) in volt. For the ends of the range the relation is not linear anymore, with -12 dB at 0.0 V and 22 dB at 1.0 V.

For the LNA all three polarisations (x, y and z) are measured. For the x and y directions, which both have two antenna arms, two inputs and one output of the VNA were used. The signal of the inputs was combined by the VNA to also know the s-parameters of the two ports together. The z direction has only one arm so one input was used. The external power source was connected via a bias-T to combine the direct current used to power the chip with the AC-coupled measurement. For the LNA the VNA was calibrated such that the s-parameters where not influenced by the connection wires and bias-T. The connections of the VNA inputs were soldered to the LNA antenna inputs.

The complete analog chain consisting of the LNA, amplifier, and filter is measured for the x, y and z direction. The connections were made in a similar way as for the separate LNAs. The calibration used for the LNA was also used for the whole chain, so the wires from the VNA to and from the devices and the bias-T were ignored, but the influence of the connection wires between the devices was not excluded from the results. The connection of the parts to each other and the VNA is shown in figure 2.2, the sequence is the same as in the antenna.

The signal was also measured by the Chinese partners of GRAND and these measurement will be compared to the ones found here in Nijmegen.

2.2 Results

The change in amplitude and in phase is measured for the analog part of the antenna. This is done for the chain as a whole and for the three different parts separately. The results of the separate parts are combined and compared to the results of the whole chain. If those results are very similar the performance of the whole chain can be known from the results of the separate parts and that makes understanding the signal much easier. In addition, when an element gets replaced, it will not be needed to repeat the measurements on the other units provided the impedances match. Furthermore, measurements done in China are compared to the results measured in Nijmegen. Below, I first look at the amplitude and afterwards the phase.

2.2.1 Amplitude Gain

For the amplitude the cutoff frequencies and the variance in the measurement region is important. The measurement region is $50 - 200$ MHz. In that region the amplification of the amplitude must be almost constant so measurements at different frequencies have the same amplification. The cutoff frequencies must lay outside the $50 - 200$ MHz range and the transition must be as steep as possible. Outside the cutoff frequencies the signal must be really small in comparison with the signal inside, because the chip that digitises the data is clocked at 500 MHz, signals at frequencies above 250 MHz are mapped to lower frequencies.

The measurements of the whole chain are made for three settings of the amplifier and for the three directions of the LNA. The minimum gain used was -12 dB, when 0 V was applied to the amplifier, and the maximum 22 dB. The LNA also adds 20 dB. The maximum gain of 42 dB is not completely achieved, because a part of the power of the signal is lost in the filter. The maximum measured gain is 40.6 dB. The graphs of the measurements are given in figure 2.3a.

The graphs show that the gains stay quite constant between 50 and 200 MHz. There is however a clear difference between the lines for the x and y and the z polarisations. This is a result of the different LNA chip used for the z polarisation, as described in section 1.2.1. The y gain is a little below x for this LNA with a difference of around 0.2 dB in the frequency range used by GRAND.

For a gain of 0 dB from the amplifier (so still a gain of 20 dB from the LNA) the amplification in the frequency range between 50 and 200 MHz stays between the 19.4 and 23.5 dB for x, but covers the range of 14.2 till 23.6 dB for z. The

larger variance in the z polarisation is mostly in the range 150 till 200 MHz. There the amplification drops 9.4 dB for z, while the gain of x only drop 4.1 dB.

For the other two gain settings of the amplifier the variance in amplification is very similar. The variance at maximum gain is between 35.4 and 40.4 dB for x and 30.0 and 40.6 dB for z. At minimum gain it is between 4.8 and 9.2 dB for x and -0.3 and 9.5 dB for z. This means that these gains settings have a difference of 5 and 4.4 dB for x and 10.6 and 9.8 dB for z. At all gain settings the variance for z is around double that of x (and y).

The cutoff frequency is around 25 MHz at the left side and around 230 MHz at the right side. This is well outside the range that GRAND uses for measurement, and well within the first Nyquist zone of data sampling, as we want. At the left side it is clearly visible that the amplitude quickly decreases, for the z polarisation with around 35 dB. At the right side the decrease is slower, but the drop is larger, around 45 dB for z. The x and y polarisation decrease with around 10 dB more on the left and 5 dB more on the right. A difference of 35 dB means that the signals outside $25 - 230$ MHz is around 56 times smaller than a signal with in this range, thus realy small in comparison.

For the separate amplifier a whole range of gain settings was measured by Dániel Szálas-Motesiczky. The ones closest to the gain settings of the whole chain were chosen here. These where the gains for -10 dB as minimum, 0 dB and 20.9 dB as maximum. The LNA and filter measurements are added to this, so there are again graphs for the three polarisations of the antenna and the three amplifier settings. The results are given in figure 2.3b. This shapes looks really similar to figure 2.3a. The x and y direction are again really close and y is a little lower than x for all gain settings. The z direction differs from x and y in a similar way as in the measurements of the whole chain.

There are differences between figure 2.3a and 2.3b, namely the absolute gain, even at 0 dB amplification. For the amplifier setting of 0 dB, the x direction of the calculated combined chain is between 15.2 and 19.4 dB instead of between 19.4 and 23.6 dB as it is for the measurement of the whole chain. Both have a variance of 4.2 dB, but the values differ by 4.2 dB amplification.

For the minimum and maximum gain settings you would expect this difference to be even larger since the gain settings of the amplifier are not exactly the same. For x at maximum gain the graph stays between 35.6 and 40.4 dB. That is almost the same as the whole chain. The variance is 4.8 dB, so 0.2 dB smaller. For z at maximum gain the graph stays between 31.2 and 41.3 dB. This is around 1 dB higher than for the whole chain and the variance is 0.5 dB smaller than the 10.6 dB for the measurements whole chain. At minimum amplification x stays

between 4.6 and 9.4 dB, really similar to the measurements of the whole chain (only 0.2 dB smaller) and the variance is the same. At minimum amplification the z polarisation stays between 0.6 and 10.0 dB. This is around 0.7 dB larger than the whole chain and the variance is with 9.4 dB 0.4 dB smaller. Over all the maximum and minimum settings of the combined chain come closer to the values of the whole chain than for the setting of 0 dB. Exactly the opposite of what you would expect. A possible cause of this effect could be that the amplification was not properly set to 0 dB during one (or both) of the measurements. A proper method of removing this uncertainty would be to perform the measurements one after the other without changing the gain of the amplification.

From China we have only the measurements amplification of the complete chain. These are shown in appendix A. These amplifications measured are very similar to the measurements of the whole chain here. In addition, they are more similar to the the measurements of the whole chain here, than to the combined measurements of the separate parts. This is especially clear if you look at the amplification with 0 dB gain from the amplifier. This tells us that the measurements of the whole chain are probably correct, since they are measured twice, and that the error is in the amplifier measurements. The amplifier measurements are done on a different day than the LNA and whole chain measurements. This could be play a role in the different values for the same gain settings.

2.2.2 Phase Shift and Time Delay

Not only the amplitude, but also the phase changes with amplification of the signal. This change in phase creates different delay times for different frequencies. To preserve the shape of the signal the delay has to be constant over the whole frequency range. The change in phase was measured for the whole frequency range and from that the delay was calculated with:

$$\tau_\phi = \left(\frac{\phi}{360} \times \frac{1000}{f} \right) \tag{2.3}$$

Where τ_ϕ is the time delay of the signal in nanoseconds, ϕ is the the shift in phase and f is the frequency in MHz.[12]

The time delay is different for the whole chain and combined chain. The delays of the whole and combined chains are shown in figures 2.4a and 2.4b respectively. These graphs are focused on the delay in the range between 50 and 200 MHz. A more zoomed out version of both is shown in appendix B. The delay in the whole chain is between the -6 and 20 ns in the frequency range

used by GRAND. The delay for different gain settings of the same direction differs $0.1 - 0.2$ ns between minimum and 0 dB gain, but differs almost 1 ns between maximum gain and the other two. For the x direction this difference is even larger.

It is also visible that the delays of the directions y and z are relatively close to each other, maximally 1.5 ns apart, while the distance to x is much larger, at some places the delay of x is almost 10 ns smaller. Why there is this large difference between x and y is not clear. Both have the same LNA, amplifier and filter, so you would expect that they are very similar. The difference of x and y is also clearly visible in the phase shift measured by the VNA, see appendix B. There x is around 180 degrees lower in the whole range of 50 till 200 MHz. It could be that the connection of the poles for x to the LNA are the other way around than for y, but during the experiment the connections were detached after measuring the x polarisation for the separate LNA and where later reattached to measure x for the whole chain. The same was done for the y polarisation. Only between the measurements of the z polarisation the wires stayed attached. It is interesting that the LNA of the x polarisation would be connected the wrong way around twice and the y polarisation has no problems. The only way to check this is to perform the experiment again. It is also interesting to see that the delay of the y and z directions are close, because these have different LNAs.

When calculating the delay using the measurements of the separate parts that are added together the delay is larger, especially around 50 MHz. There the delay of the combined chain is approximately 16 ns higher. At 200 MHz, the other end of the range, the difference is much smaller. Here the measurements of the whole chain is around the 1 ns smaller. The range of the delay calculated from the measurements of the individual parts is therefore larger than that measured with the whole chain. It should be noted that reflections have not been taken into account in the calculations. Even though these are expected to be small, they may cause differences in comparison to the measurements of the full chain.

2.3 Conclusion

The amplitude amplification is quite constant with in the range used by GRAND ($50 - 200$ MHz) and outside this range the amplification of the amplitude is cut off around 25 and 230 MHz. At the cutoffs the amplification decreases quickly, as was intended. There is a difference in the amplification of the x and y, and the z polarisation. This is the result of the different chip used for the z polarisation.

There is a difference between the measurements of the whole chain and the

measurements of the separate part that are later combined. This difference is especially clear at a setting of 0 dB for the amplifier (thus still a amplification of 20 dB from the LNA). Where this difference comes from is unclear. The Chinese measurements are also known and these are similar to the measurements of the whole chain done here in Nijmegen. This suggests that the fault is in the measurements of the separate parts.

From the phase shift of the signal the delay is calculated. For most part of the range of GRAND the delay does not differ a lot, which is good. The x polarisation is quite far apart from the y and z polarisation. This is surprising, because the x and y polarisation have exactly the same circuit. The difference between the measurements of the whole circuit and the measurements of the separate parts that are combined are very similar. The difference is larger around 50 MHz and almost non existing around 200 MHz.

To know what happened in the experiments to create these differences between the measurements of the whole chain and the measurements of the separate parts the experiments have to be done again to see if a mistake was made in the connections or measurements.

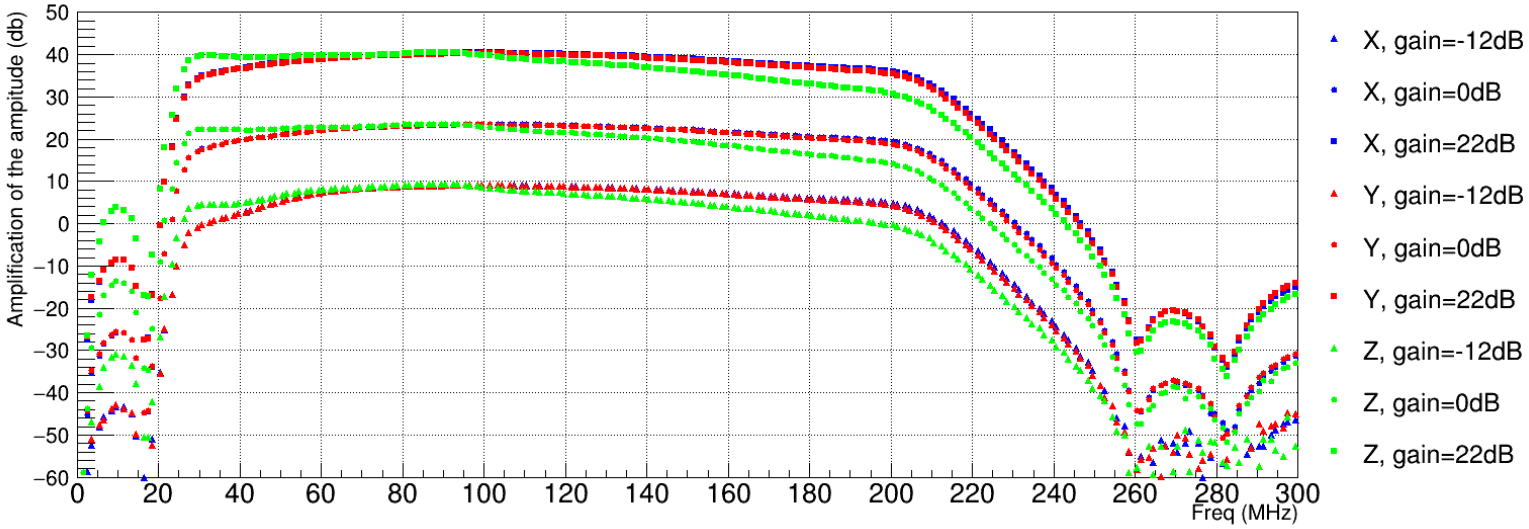

(a) Gain in amplitude from the measurements of the whole chain.

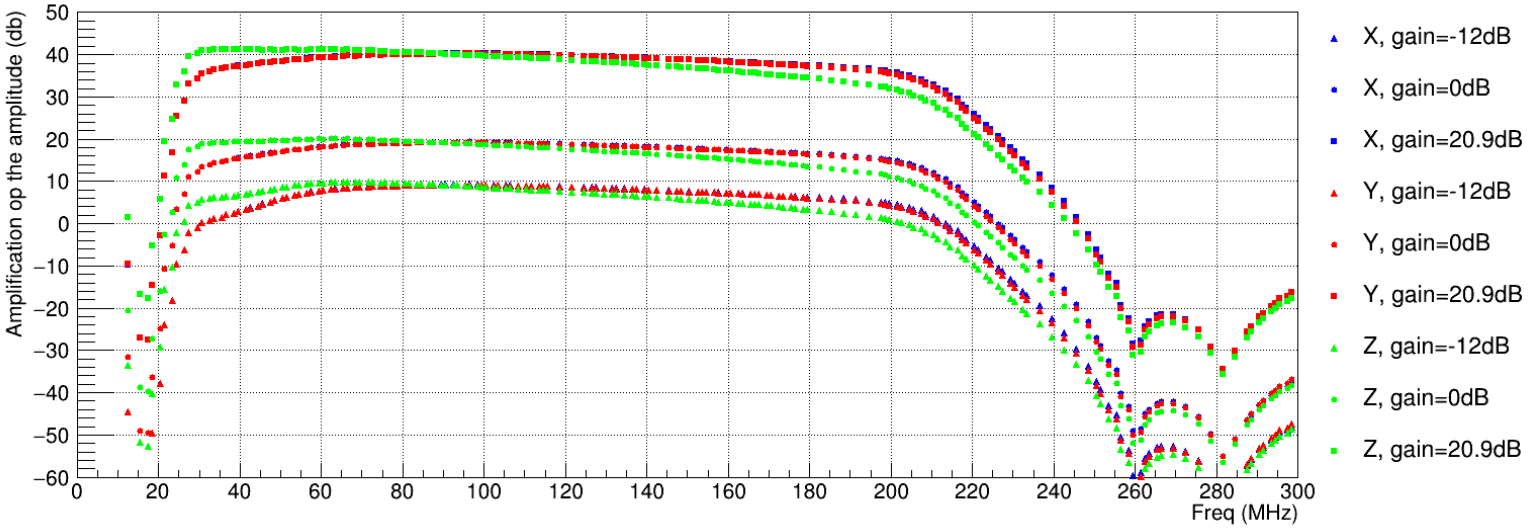

(b) Gain in amplitude from the measurements of separate parts combined.

Figure 2.3: (a) The gain of the amplitude as measured with the whole chain. The amplification is measured for the three directions of the antenna (x, y and z) and for the maximum, zero and minimum gain of the amplifier. The LNA caused a constant gain of 20 dB. (b) The gain of the amplitude from the added values of the separately measured parts. The amplification is calculated for the three directions of the antenna (x, y and z) and for the maximum, zero and minimum gain of the amplifier. This time the minimum was -10 dB, not -12 dB, because that was the lowest measured gain of the amplifier. The LNA again caused a constant gain of 20 dB.

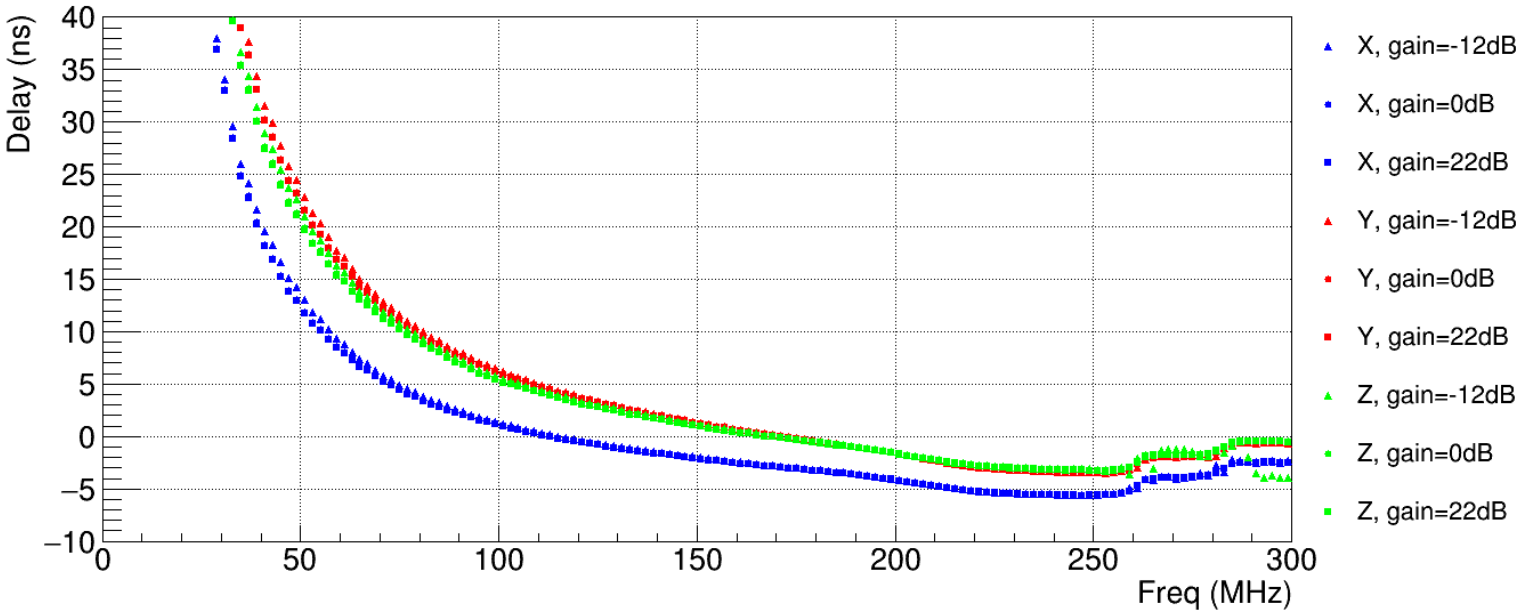

(a) Delay measured by the whole chain

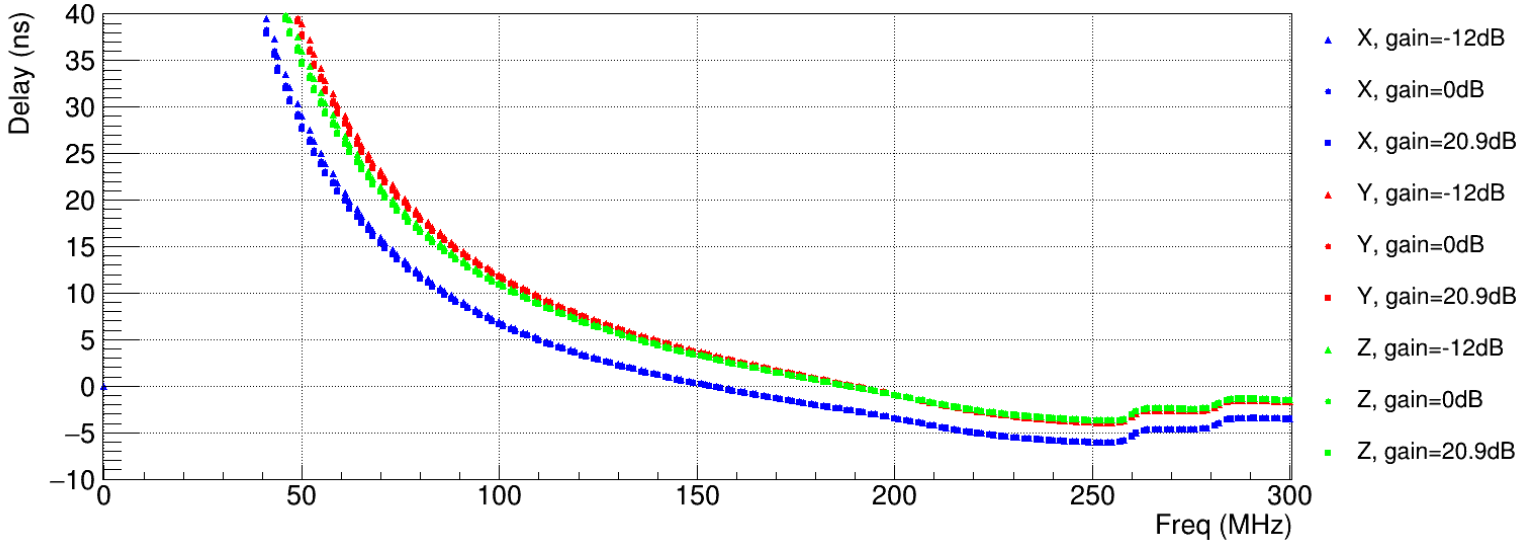

(b) Delay measured by the combined chain

Figure 2.4: (**??**). The time delay measured in the whole chain. The measurement of the three directions and three gain settings are shown here. (**??**) The time delay measured in the combined chain. The phase shift of all parts is first added together and the total is used to calculate the delay of the combined chain.

3 | Analysis of the Cosmic Ray induced Air Shower Signal

3.1 Method

The ZHAires air shower simulation package is used to create showers of a number of cosmic rays. For this analysis five such cosmic rays are used which have a zenith angle of 51.8° and an energy of $3.98 \cdot 10^{18}$ eV. All arrive directly from the North. However, the depth of the shower, X_{max}, is different for these five cosmic ray showers. The lowest value is 711.23 g/cm^2 and the highest (thus deepest shower) is 853.42 g/cm^2. For each shower we have created a histogram for each antenna of GRAND with the received electromagnetic signal that such an air shower produces. The signal received by the x, y and z direction of the antenna are all put in separate histograms. The three polarisations are also squared and combined in another histogram so each antenna of GRAND has four histograms for one cosmic ray. The histograms of all antennas are put together in a ROOT file.[i] The position of each antenna is given by the angle θ, which is the opening angle between the shower axis and the line between the position of shower maximum and the antenna position, and ψ, the angle between the projection of the shower axis on the ground and the line between the shower core and the antenna, see figure 3.1. These files are used in this research to look for a relation between the duration of the signal received by the antennas and the X_{max} of the shower. Using

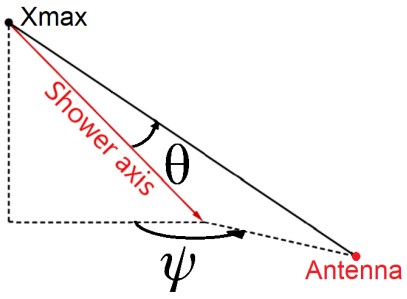

Figure 3.1: The position of the antenna relative to the shower axis is given by the angles θ and ψ. θ is the angle between the shower axis and the line from X_{max} to the antenna, and ψ is the angle between the projection of the shower and the line from the shower core to the antenna.

[i] A certain type of file that is used by the programming framework ROOT from CERN.

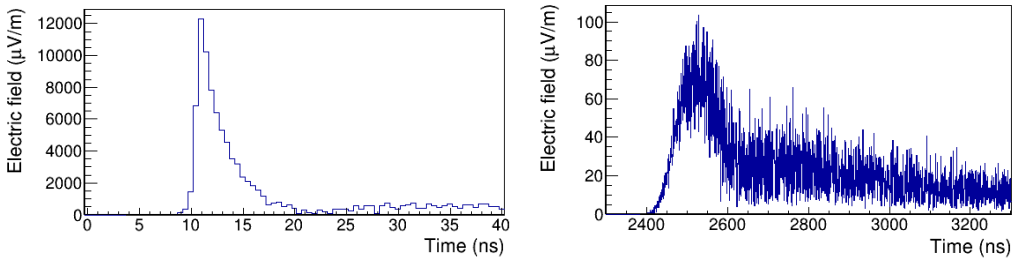

(a) Histogram of an antenna at a small angle $\theta = 2.2$ degrees.

(b) Histogram of an antenna at a large angle $\theta = 12.4$ degrees.

Figure 3.2: Two histograms of two different antennas, one at a position with a small θ and one at a position with a large θ. Both have $\psi = -90$ degrees and $X_{max} = 756.97$ g/m^2.

such a relation, the duration can give information about the nature of the primary particle.

In this analysis, only the histograms with the information of the three polarisations added together are used and only the histograms of the antennas outside the Cherenkov angle. At the Cherenkov angle the width of the peak of the signal is close to 0 ns independent of the shower development, therefore these are not useful for this research. Using only these antennas there are 127 positions left, thus there are 127 histograms per ROOT file. For these histograms the full width at half maximum (FWHM) is calculated. This is the width of the peak at half its height. The FWHM is calculated in two ways. The first method is to get the FWHM directly from the data. The maximum is given by the height of the peak and the locations where the values cross half this maximum give the FWHM. For the left side we use the value where the histogram first reaches the half maximum value and for the right side where the histogram first falls below that value.

However, this method has a few problems. For antennas near the Cherenkov angle the slope at the left-hand side of the peak is so steep that it only spans one or two bins of the histogram. As a result the bin with a content above the half maximum is often the same bin as the bin with the maximum value, see figure 3.2a. For antennas far away from the shower core the noise is much larger in comparison to the signal, see figure 3.2b. Consequently, the maximum value is no longer simply the height of the peak. It makes it harder to find the FWHM, especially on the right-hand side of the peak, as the noise makes the values of bins drop below the half maximum value sooner than the signal would fall below

that value. This is less a problem on the left-hand side of the peak because the fluctuations are less.

The second method to find the FWHM is to fit the histograms in the ROOT file first and than find the x values for which the fit is at half its maximum. This solves the problem of too few bins for small angles and would help with the large noise for larger angles.

For this second method two fit functions are tried using ROOT from CERN. The fit functions are the Gaussian function and the Landau distribution. The Gaussian fit function, equation 3.1, has three parameters, the multiplication a, the mean μ and the sigma σ. Before the fit the parameters are set at start values, these were chosen to be the maximum of the histogram for a, the x value of the maximum for μ and the $\sigma = 10$.

$$g(x) = a \exp\left(-\frac{(x-\mu)^2}{2\sigma^2}\right) \tag{3.1}$$

The Landau fit function is given by equation 3.2 with $\lambda = (x-\mu)/\sigma$. This function has the same three parameters as the Gaussian, with again a set at the maximum and μ set at the x value of the maximum, but this time $\sigma = 1$.

$$l(\lambda) = \frac{a}{2\pi i} \int_{c-i\infty}^{c+i\infty} e^{\lambda s + s\log s} ds \tag{3.2}$$

The error of the FWHM is calculated in the same manner for both fit functions. It uses the relative error of the maximum e_{rel} of the fit. This is calculated as

$$e_{rel} = \sqrt{\frac{\chi^2}{NDF}} \frac{e_a}{a}. \tag{3.3}$$

If $\frac{\chi^2}{NDF} < 1$ it is set to 1. $\frac{e_a}{a}$ gives the relative magnitude of the error e_a of the parameter a of the fit (see equations 3.1 and 3.2). χ^2 is a measure of the difference between the fit and the data and NDF is the number of degrees of freedom of the fit.

The definition of χ^2 used by ROOT is

$$\chi^2 = \sum \frac{\left(y - f(x)\right)^2}{e_y^2 + \left(\frac{1}{2}(e_{xl} + e_{xh}) f'(x)\right)^2} \tag{3.4}$$

Where y is the content of the bin and $f(x)$ is the value of the fit. The square of this difference is divided by the square of the y error (e_y) and the square of contribution

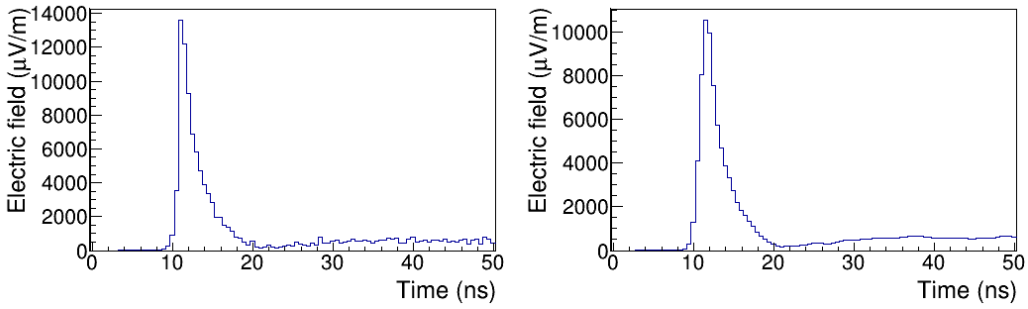

(a) Not smoothed.

(b) Smoothed.

Figure 3.3: The smoothed and not smoothed signal received by an antenna. The antenna is at $\theta = 2.04$ and $\psi = -90$ and the depth of the shower is $X_{max} = 711.23$ g/cm^2.

of the error of x. This way of calculating the error is called the effective variance method. It only works if the errors in x and y are independent. The contribution of the error of x is given by $\frac{df(x)}{dx}e_x$ (for small errors). For the error of x ROOT uses the combination of the high x (e_{xh}) and the low x (e_{xl}) of the x-bin. For e_y ROOT chooses between the high or low error depending on if the fit lies above or below the data.[13,14] The error of y is the error of the measurements and error of x is half the width of the bins, in our case this width is 0.5 nanoseconds. The error of x is thus on both sides the same so $e_{xh} = e_{xl}$.

A new half maximum value $(1 + e_{rel})max_{fit}/2$ is calculated and a new width using the fit at that height. The difference between this new width and the normally calculated FWHM is used as the error of the FWHM.

It turns out that the noise is not only a problem for the first direct method, but also for fitting the data in the second method. The end point of the fit has to be set at the end of the first peak to get a good Gaussian of Landau fit, but it is hard for a program to properly determine this point. Setting the end point too close and the fit does not fall below the half maximum, therefore the FWHM can not be calculated. Setting the end point too far and the fit doesn't follow the first peak and becomes very low and wide, which makes the FWHM very large and incorrect. To make it easier to find the end point the curve is smoothed. This however deforms the data, so the fit is still performed on the original data.

This smoothing of the of the peak can also be used by the fist method. Here the change of the data has more consequences, because the FWHM is given directly by the smoothed data. The smoothing function of ROOT uses the neighbouring

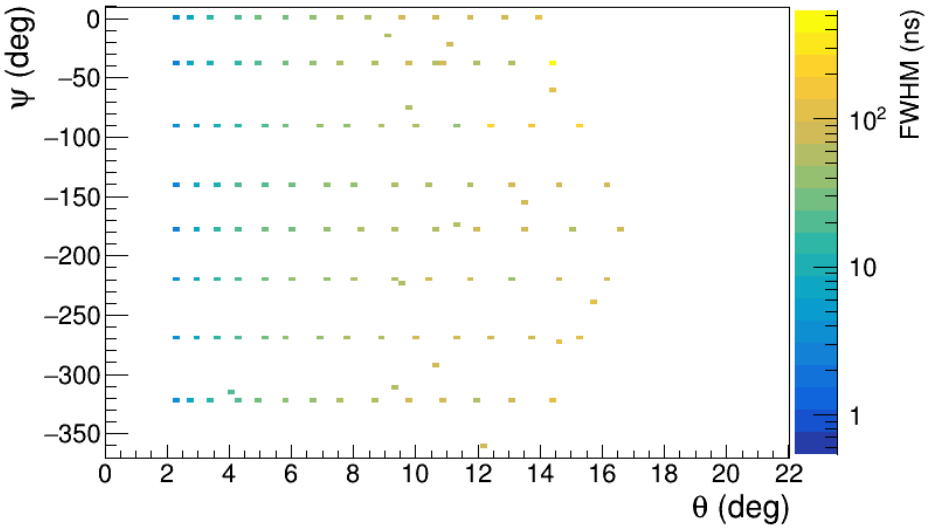

Figure 3.4: The FWHM against the ψ and θ for a cosmic ray with depth 711.23 g/m^2. This plot is made with the FWHM calculated directly from the data.

points to create a new value for each bin. This could create a problem for the peaks at lower angles, because these peaks exist of only a view bins. The result of such smoothing can be seen in figure 3.3. The peak becomes lower, which increases the FWHM. In some cases this can double the FWHM. For higher angles the data has to be smoothed in order to improve it enough to find the FWHM with the first method. However, this would make the FWHM at lower angles a lot less reliable.

The fist method already indicated that the angle ψ does not have much influence on the width, but θ does. This is shown in figure 3.4. The plots for the other four depths are very similar and can be found in appendix C. The results therefore focus mainly on the relation between the FWHM and θ and how this is influenced by changes in X_{max}.

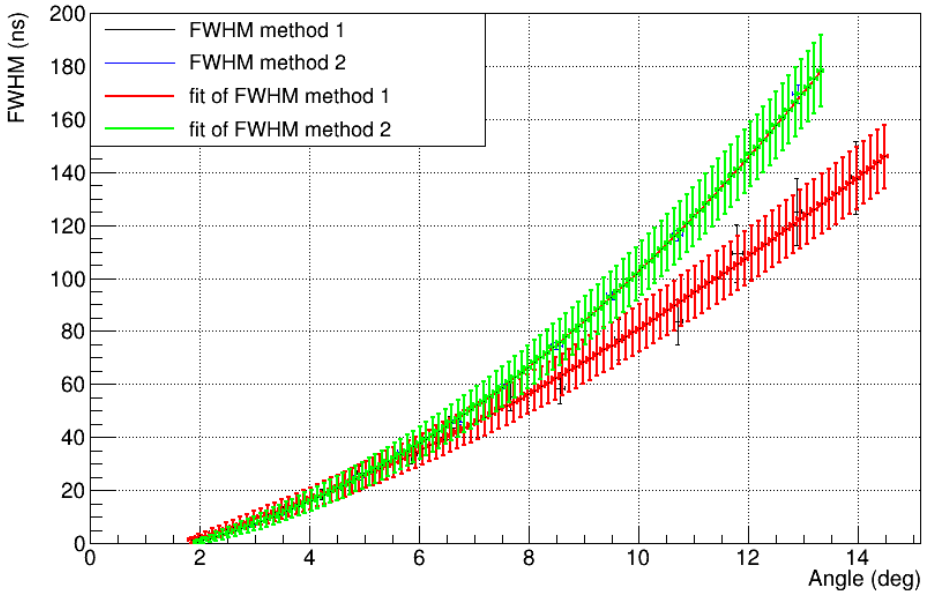

Figure 3.5: The results of the two different methods to calculate the FWHM at a depth of 757.8 g/cm^2 and $\phi = 0$. The fit used for the second method is the Landau fit.

3.2 Results

The calculated FWHM differs depending on the method used and on which of the two fit functions in the second method is chosen. The results of method 1 and method 2 with the Landau fit are shown in figure 3.5. This is only for $X_{max} =$ 757.8 g/cm^2 and $\psi = 0$ degrees, but the difference between the two methods looks similar for the other values of X_{max} and ψ. The FWHM values of the two methods are close for θ angles smaller than 8 degrees, but for larger angles the results diverge. This is also where the noise plays a much larger role.

The two fit functions used to calculate the FWHM, the Gaussian and the Landau, both have advantages and disadvantages. The Landau gives a better fit for the smaller θ angles where the peak is less symmetrical and smaller. For the higher θ the peak becomes lower and wider and more symmetrical and as a result the Gaussian fit works better than for lower θ, but still not perfect. The Gaussian FWHM is often too small, but it better describes the height of the peak than that

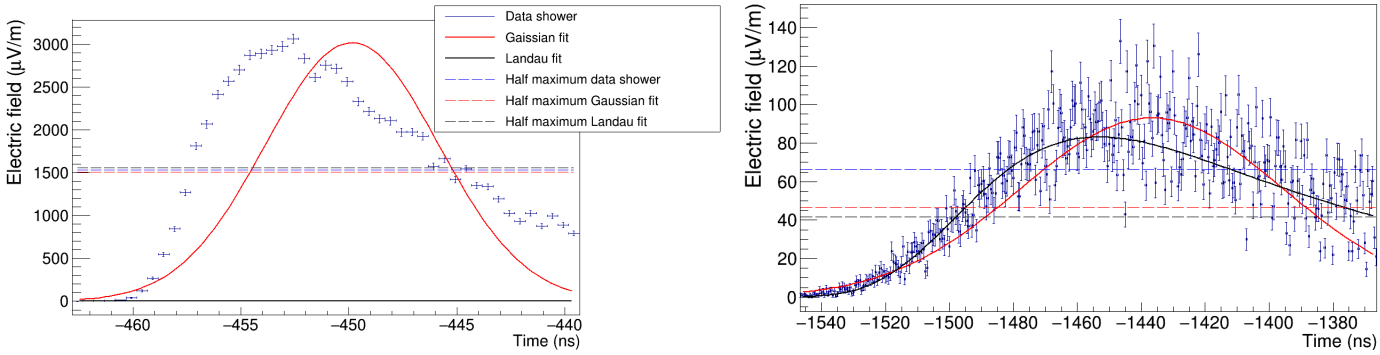

(a) $\theta = 3.6$ degrees

(b) $\theta = 13.1$ degrees

Figure 3.6: The Gaussian and Landau fit at a low and high value for θ. The depth of the shower is $X_{max} = 756.97$ g/cm^2 and $\psi = -218.2$ degrees. The half maximum is half of the highest value. If the noise creates high values the half maximum line of the data lies high compared to the fits.

the Landau fit. The Landau follows the data better (except at the top), but becomes wider than the data for the higher angles. It also has the problem that it does not always drop below half its maximum value at the right-hand side of the fit. This happens when the Landau fit is just above his half maximum so the FWHM is determined by using the right boundary of the fit, but this is of course less precise. Therefore these FWHM values are not used in the results. Both fits will be used to investigate how the depth influences the FWHM.

Once the FWHM values are calculated and plotted against the θ angles, this is fitted with a third degree polynomial function. Figures 3.7 and 3.8 show two times four graphs of the FWHM against the angle θ for three of the five depths. The four graphs are at the locations right below the shower axis ($\psi = 0$), on both sides of the shower ($\psi = -90$ and $\psi = -270$) and on the opposite of the arrival direction ($\psi = -180$). Only three depths are shown here for clarity. The other two depths fall between 711.23 and 757.8 g/cm^2 and their fits fall between the fits of 711.23 and 757.8 g/cm^2. This makes it hard to distinguish them, and thus they are left out. The graphs with all five traces are given in appendix D.

The vertical black line gives the maximum θ angle for which the FWHM can be calculated. The difference where the black lines are drawn is partly due to the fact the ROOT files with the data do not all have the same maximum value of θ. The file with $X_{max} = 711.23$ g/cm^2 has a maximal $\theta = 14$, 757.8 g/cm^2 has its

maximum angle $\theta = 16$ degrees and 853.42 g/cm^2 has a maximum $\theta = 21$. If the graph stops at a lower angle than these, it means that all fits of the data at higher θ did not fall below the half maximum on the right-hand side. The black lines are at lower values θ for the Landau fits than for the Gaussian fits. This corresponds to the problem of the Landau described above.

The forms of the fits of the FWHM vs the θ angle of the Gaussian and Landau method look similar for the same ψ, as would be expected since both methods are good fits of the data. Where the fits of the two methods differ is for the maximum angle θ at which the FWHM is calculated. Below the maximum they are the same and it is after this maximum angle that they behave very differently. For different ψ values within one fit method the differences are larger, though not as large as the differences for changing θ angles. The FWHM vs angle fit for $\psi = 0$, right below the shower, it is more curved upward while at $\psi = -180$, opposite of the shower, is more straight. This difference is larger for the FWHM calculated with Landau than with the Gaussian fit. The difference can be as large as tens of nanoseconds, hence the ψ angle can not be ignored in determining the X_{max} from the signal width.

To deduce the X_{max} from a shower, only the fits at θ angles below the maximum θ can be used. The fits at a smaller θ are also better. If the FWHM becomes too large the peak is difficult to distinguish from the noise. This is probably not a real problem here, because the FWHM stays below 100 ns for the range of θ that we are interested in, see below. The differences must also not be too small, since GRAND has a sampling frequency of 500 MHz. That means that it can only distinguish differences in width if they are larger than $1/500$ MHz $= 2$ ns. Peaks with a width smaller than 2 ns are also not always detected. It is possible to have a peak that is wider than 2 ns with a FWHM that is smaller. Taking the FWHM higher than 2 ns however is a easy way to ensure that the peak can be detected. Since there are enough peaks with wider FWHMs, the restriction that FWHM can not be smaller than 2 is used here. To say more about which θ angles are good for distinguishing the values of X_{max}, we have to look at specific fit functions and ψ angles. For the Gaussian fit these results are shown in table 3.1 and for the Landau fit in table 3.2. The first column gives the two X_{max} for which the fits are compared and the second the difference ΔX_{max}. The last four columns show the minimum angle θ for which the fits of the depths are more than 2 ns apart. For θ greater or equal to this angle the diffidence can be measured. The third column shows the minimum angle θ for which the difference between the fits can be measured in all directions of ψ.

The smallest angle is not only determined by the distance between the fits, but

Compared X_{max} (g/cm^2)	ΔX_{max} (g/cm^2)	all ψ	$\psi = 0$	$\psi = -180$	$\psi = -90$	$\psi = -270$
711.23 - 853.42	142	2.4	2.4	2.4	2.5	2.3
757.8 - 853.42	116	3.5	2.9	2.9	2.9	3.5
737.41 - 853.42	116	2.9	2.4	2.7	2.5	2.9
737.41 - 757.8	96	5.6	4.5	5.6	5	4.2
756.97 - 853.42	96	3.1	2.4	3.0	2.7	3.1
711.23 - 757.8	47	3.9	3.8	3.9	2.8	3.0
711.23 - 756.97	46	4.5	4.3	3.2	4.5	3.4
711.23 - 737.41	26	6.3	5.5	5.2	3.2	6.3
737.41 - 756.97	20	–	5.0	4.5	–	5.7

Table 3.1: The minimum values of θ for which the two compared values of X_{max} can be distinguished. The FWHM is calculated with the Gaussian fit. The minimum values are in degrees and the ψ tells for which ψ angle the minimum values apply. The difference between 756.97 and 757.8 g/m^2 is left out, because these values of X_{max} are to close together.

Compared X_{max} (g/cm^2)	ΔX_{max} (g/cm^2)	all ψ	$\psi = 0$	$\psi = -180$	$\psi = -90$	$\psi = -270$
711.23 - 853.42	142	2.5	2.4	2.5	2.5	2.4
757.8 - 853.42	116	2.9	2.4	2.9	2.9	2.4
737.41 - 853.42	116	2.7	2.5	2.7	2.3	2.1
737.41 - 757.8	96	5.2	4.7	5.2	5.2	4.7
756.97 - 853.42	96	2.9	2.4	2.9	2.6	2.5
711.23 - 757.8	47	4.0	4.0	3.0	2.6	3.3
711.23 - 756.97	46	3.6	3.6	2.9	3.6	3.3
711.23 - 737.41	26	4.3	4.3	3.8	3.9	4.2
737.41 - 756.97	20	5.7	5.2	4.9	5.7	5.7

Table 3.2: The same kind of table as for the Gaussian fit, only now the FWHM are calculated with the Landau fit.

also by the size of the FWHM since these to have to be larger than 2 ns. This only plays a role for $\Delta X_{max} = 142.19$ g/cm^2. For angles of around $\theta \leq 2.5$ the fit of 853.42 g/cm^2 drops below 2 ns. For the Gaussian fit this did not have an influence. For the Landau fit the lowest allowed θ was pushed up a few tenth of a degree by this restriction. Comparing the two tables shows that the minimum allowed θ angle does not differ much for the both fit methods. The values of the the Gaussian fit are a little higher and for 737.41 and 756.97 g/cm^2 the fits are never more than 2 ns apart. The maximum usable angle θ for all angles ψ does vary. For the Gaussian fit this would be 11 degrees and for the Landau fit is this only 8 degrees (see the graphs of all five values of X_{max}). To obtain a precision of X_{max} of 26 g/cm^2 the angles $6.3 \leq \theta \leq 11$ are usable for the Gaussian method and for the Landau method a precision of 20 g/m^2 can be obtained between the angles $5.7 \leq \theta \leq 9$. This all is without the error of the fit of the FWHM vs θ.

For the Gaussian method the errors of the X_{max} fits at $\psi = 0$ degrees and angle $\theta = 9$ degrees are 9 ns for $X_{max} = 711.23$ g/cm^2, 8 for $X_{max} = 737.41$ g/cm^2, 756.97 g/cm^2 and 757.8 g/cm^2, and 7 ns for 853.42 g/cm^2. The difference between the fits of most distant X_{max} values 711.23 and 853.42 g/cm^2 ($\Delta X_{max} = 142.19$ g/cm^2) is 30.5 ns, thus more than 3σ. For the smaller differences in X_{max} values such as 737.41 and 853.42 g/cm^2 ($\Delta X_{max} = 116.01$) the difference between the fits is 23.1 ns, a little less than 3σ. For X_{max} values 756.97 and 853.42 g/cm^2 ($\Delta X_{max} = 69.45$) it is the same, 23.1 ns. The difference between 737.41 and 756.97 g/m^2 ($\Delta X_{max} = 19.56$) is almost zero for this ψ value. For the values 757.8 and 853.42 g/cm^2 ($\Delta X_{max} = 95.45$) the difference is 17.4 ns, thus more than 2σ. For the values 711.23 and 757.8 g/cm^2 ($\Delta X_{max} = 46.57$) the difference is 13.1 ns, only 1σ. All other differences in X_{max} values (these have $\Delta X_{max} \leq 45.74$) have less then 1σ difference between the fits at $\theta = 9$ degrees.

The Landau method at $\psi = 0$ degrees and angle $\theta = 9$ degrees creates fits that have the errors 9 ns for 711.23 g/m^2, 10 ns for 737.41 and 756.97 g/m^2,and 8 ns for 757.8 and 853.42 g/m^2. If we again look at the differences between the fits, these are mostly larger. The difference of 711.23 and 853.42 g/cm^2 ($\Delta X_{max} = 142.19$ g/cm^2) is 38.5 ns, thus 4σ. 737.41 and 853.42 g/cm^2 ($\Delta X_{max} = 116.01$) have a difference between the fits of 31.5 ns, thus 3σ. And for X_{max} values 756.97 and 853.42 g/cm^2 ($\Delta X_{max} = 69.45$) the difference is 25.8 ns, a difference of more than 2σ. For the values 757.8 and 853.42 g/cm^2 ($\Delta X_{max} = 95.45$) the difference is 22.8 ns, again more than 2σ. For the values 711.23 and 757.8 g/cm^2 ($\Delta X_{max} = 46.57$) the difference is 15.7 ns, above 1σ. And last 711.23 and 756.97 g/cm^2 ($\Delta X_{max} = 45.74$) have a difference of 12.7 ns, above the 1σ again.The difference between the other fits ($\Delta X_{max} \leq 26.18$ g/cm^2) of X_{max} values fall below 1σ

Gaussian fit of the peak

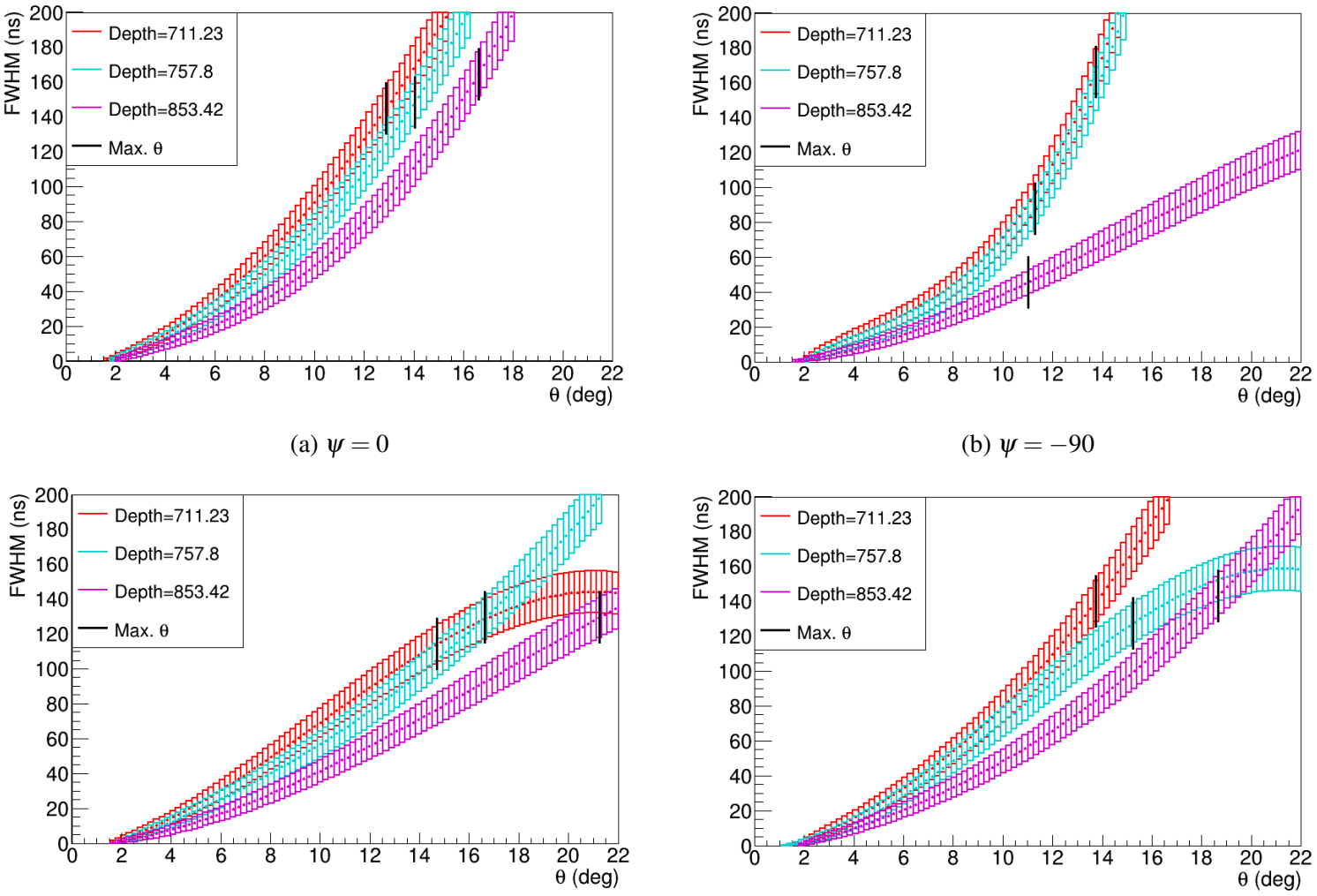

(a) $\psi = 0$

(b) $\psi = -90$

(c) $\psi = -180$

(d) $\psi = -270$

Figure 3.7: The fits of the FWHM vs the angle θ with the FWHM from the Gaussian fit of the data.

Landau fit of the peak

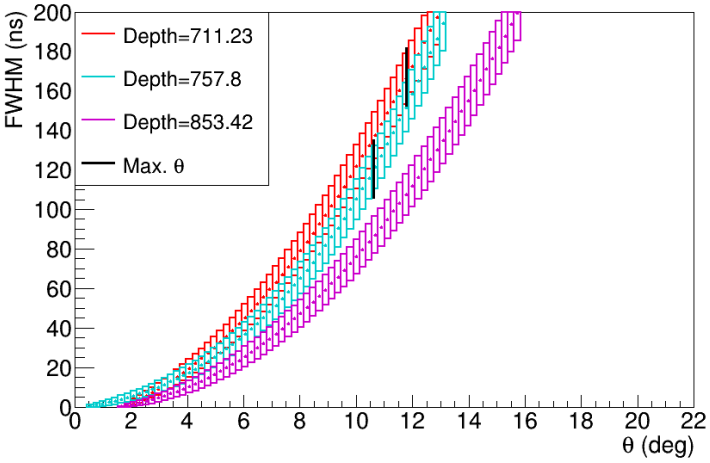

(a) $\psi = 0$

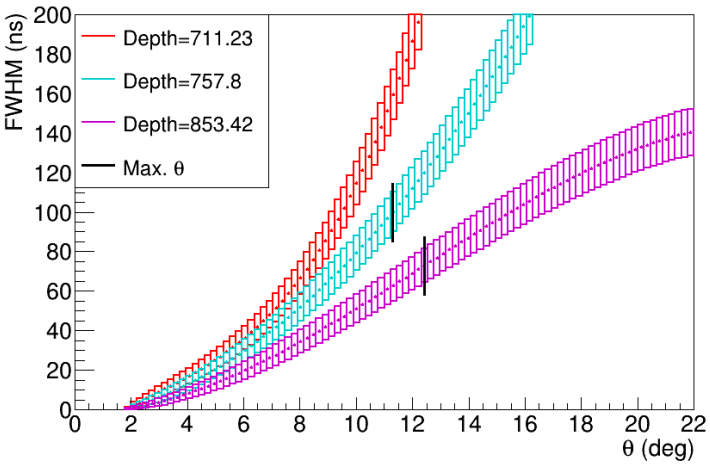

(b) $\psi = -90$

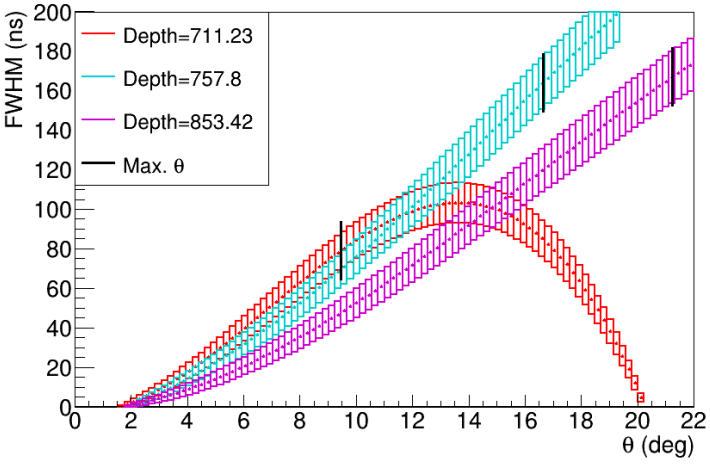

(c) $\psi = -180$

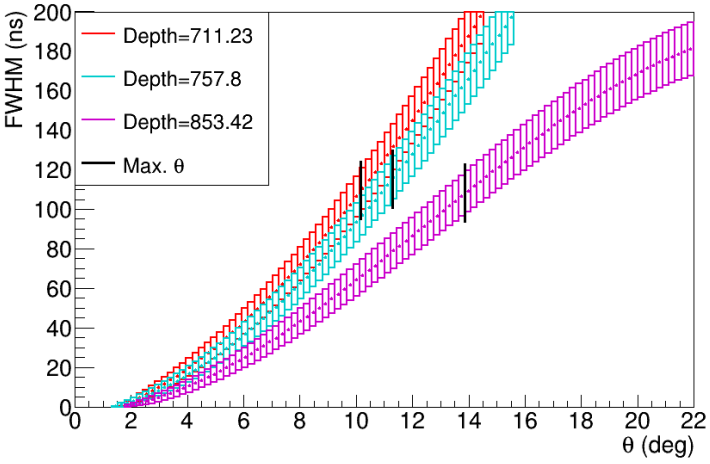

(d) $\psi = -270$

Figure 3.8: The fits of the FWHM vs the angle θ with the FWHM from the Landau fit of the data.

3.3 Conclusion

The dependence op FWHM on θ is much larger than the dependence on ψ, but the dependence on ψ is still there. To determine the value of X_{max} ψ can therefore not be ignored. To find the differences in X_{max} the FWHM has to be plotted against θ for each ψ separately.

Which fit method is best depends on the θ angle. Looking at the θ at the low end of this range the Landau fit is the best to calculate the FWHM, as it follows the peak better, though the height of the peak is often a little low. The X_{max} can also be distinguished for a lower θ angles, see table 3.2. At the high end of the range the Gaussian fit is better, because it has less problems with the shape of peaks at higher θ angels and therefore can still calculate FWHM at angles higher then $\theta = 9$ degrees.

Which angles of θ can be used variate with ψ, but the ranges $6.3 \leq \theta \leq 11$ for the Gaussian method and $5.7 \leq \theta \leq 9$ for the Landau method can be used for all ψ. These give a precision of X_{max} of 26 g/cm^2 and 20 g/cm^2 respectively. This is without the error of the fit. With this range in θ angles there are enough antennas to contribute and therefore it should be possible to distinguish X_{max} with a precision of of around 25 g/m^2.

If the errors are added and we look at the graphs for $\psi = 0$ and $\theta = 9$ this gives how many σ the different X_{max} values are apart and thus how significant the difference is that can be measured. For the Gaussian fit the difference in X_{max} can thus be distinguished with a significance of 1σ with a precision of around 45 g/m^2. For the Landau fit this is a precision of around 25 with the same significance. The Landau method seems to have a better precision for the same θ, but the Gaussian method allows higher angles of θ. At higher angles the distance between the graphs becomes larger and the error not that much.

With both fit methods the difference between an iron nucleus and a proton ($\Delta X_{max} = 100$ g/cm^2) can definitely be found and even the difference with lighter nuclei. How much of this difference is still significant with the extra noise from the antenna remains to be seen, but with the large difference between the maximum and minimum X_{max} values it seems reasonable that a proton and iron nucleus can still be disguised afterwards.

Bibliography

1. Gaisser, T. K., Engel, R. & Resconi, E. *Cosmic Rays and Particle Physics* 2nd (Cambridge University Press, 2013).
2. Schröder, F. G. Radio detection of cosmic-ray air showers and high-energy neutrinos. *Progress in Particle and Nuclear Physics* **93,** 1–68 (2017).
3. Matthews, J. A Heitler model of extensive air showers. *Astroparticle Physics* **22,** 387–397 (2005).
4. Sommers, P. Experimental aspects of cosmic rays. *ResearchGate,* 177–190 (2006).
5. Álvarez-Muñiz, J. *et al.* The Giant Radio Array for Neutrino Detection (GRAND): Science and design. *Science China Physics, Mechanics & Astronomy* **63,** 1674–7348 (2019).
6. Huege, T. & Besson, D. Radio-wave detection of ultra-high-energy neutrinos and cosmic rays. *Progress of Theoretical and Experimental Physics* **2017,** 387–397 (2017).
7. Huege, T. Radio detection of cosmic ray air showers in the digital era. *Physics Reports* **620,** 1–52 (2016).
8. Timmermans, C. *Using the Radio Cherenkov-angle.* Not published. 2020.
9. Engels, A. *et al. The antenna system for GRANDProto 300.* Not published. 2021.
10. Horowitz, P. & Hill, W. *Elektronica kunst & kunde, deel 1: analoge technieken* (Uitgeverij Sigment B.V., Beek, 1996).
11. Tektronix. *Introduction to VNA Basics.* `https://www.tek.com/document/primer/introduction-vector-network-analyzers-basics`. 2017.
12. Merlijn van Veen. *GROUP DELAY 101.* `https://www.merlijnvanveen.nl/en/study-hall/165-group-delay-101`. Consulted 03-05-2021.

13. ROOT Reference Guide. *TGraph Class Reference* https://root.cern/doc/master/classTGraph.html\#aa978c8ee0162e661eae795f6f3a35589. Consulted 07-01-2021.

14. Physics Libretexts. *Fitting Techniques*. https://phys.libretexts.org/Learning_Objects/Demos_Techniques_and_Experiments/Fitting_Techniques. Consulted 07-01-2021.

A | Antenna Measurements from China

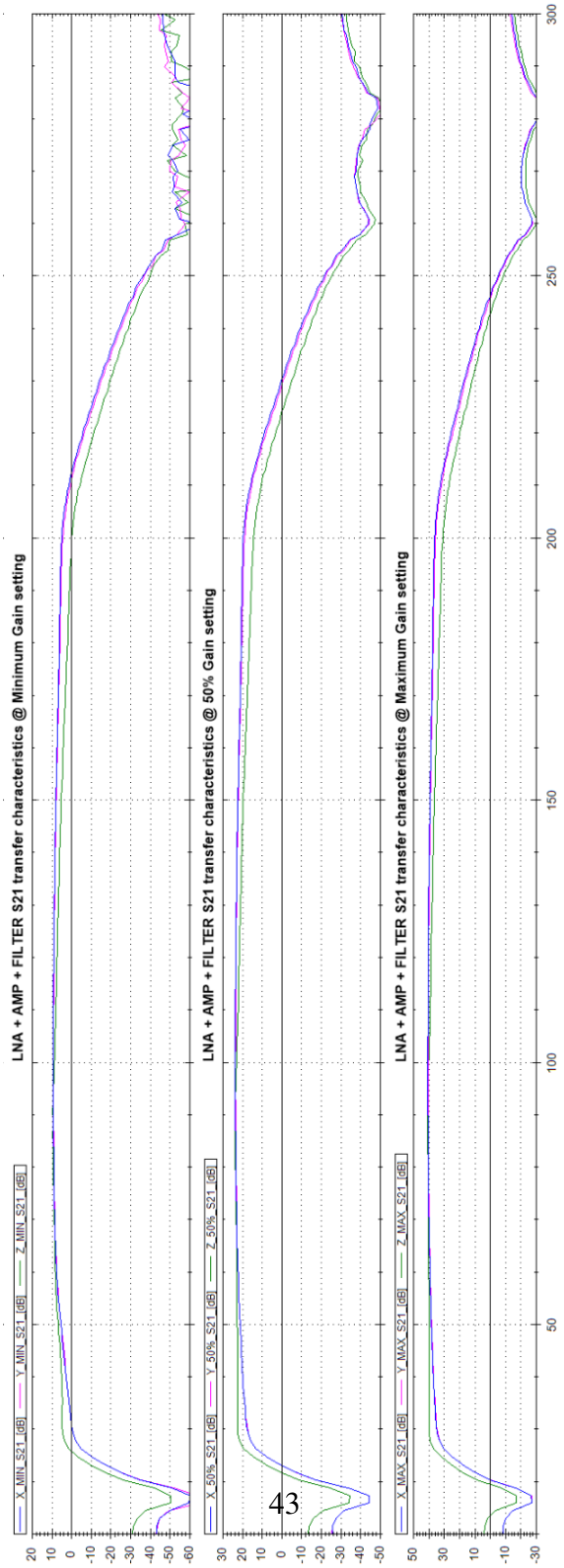

Figure A.1: The measurements of the of the amplification for the whole chain executed in China. Only these graphs are available so unfortunately their shape and text size cannot be changed.

B Extra Figures Antenna Measurements

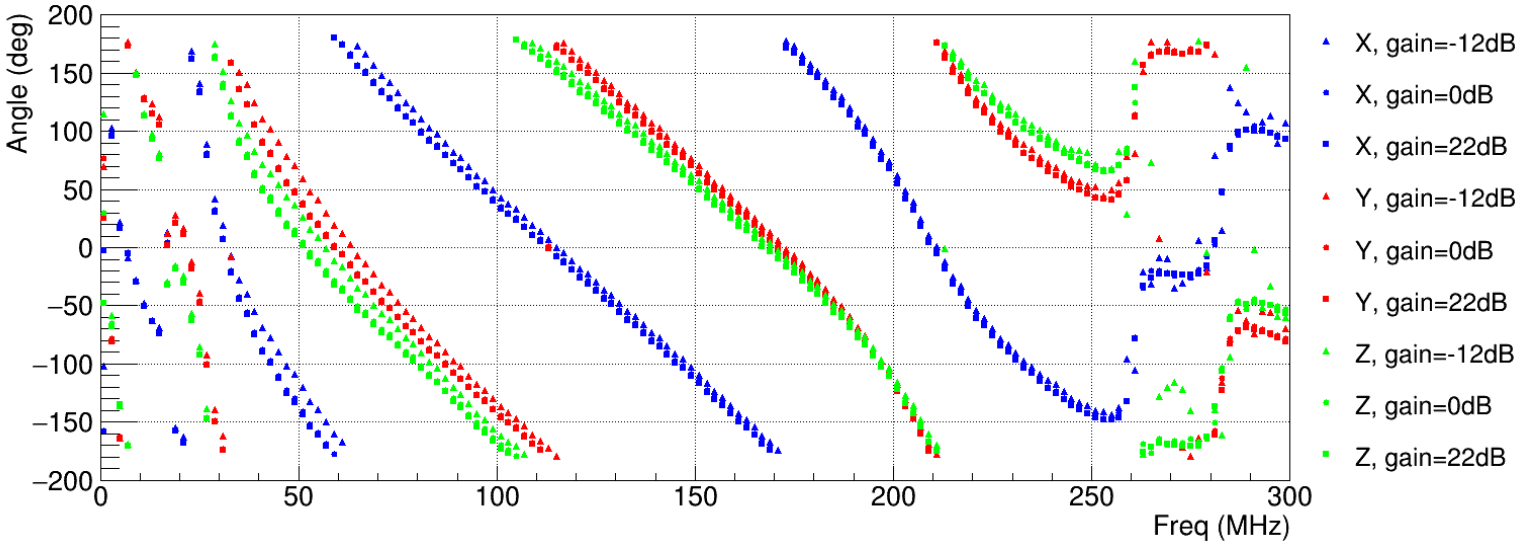

(a) Phase shift of whole chain

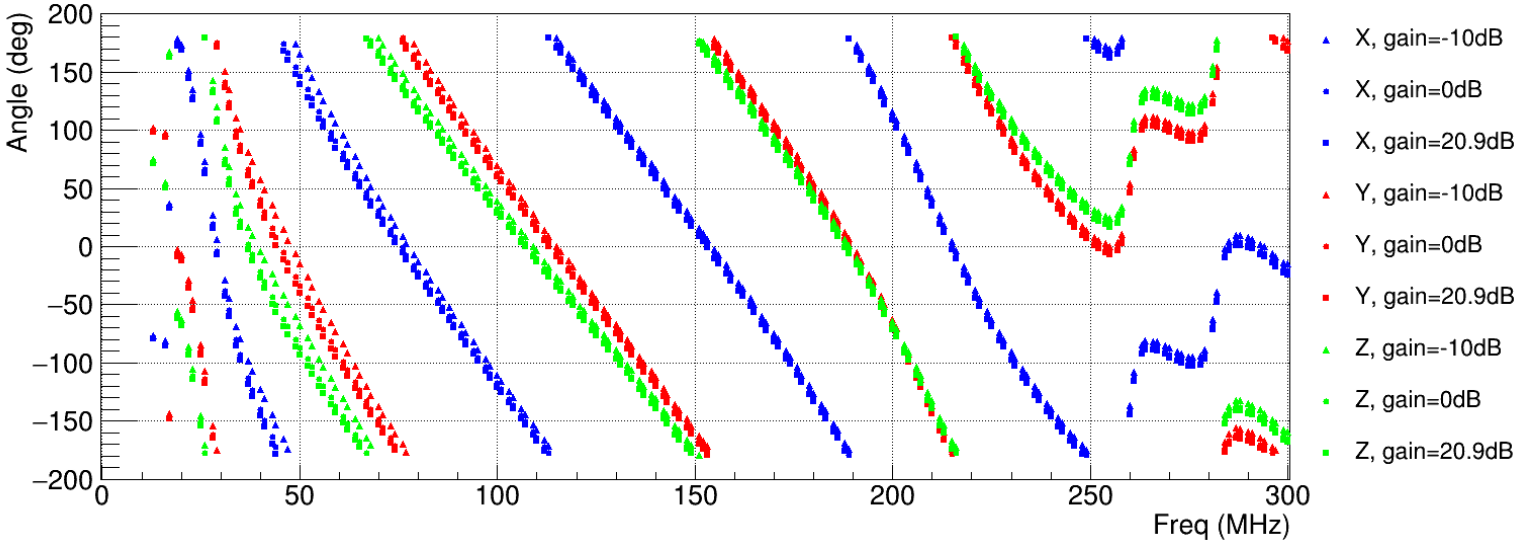

(b) Phase shift of the separate parts combined afterwards.

Figure B.1

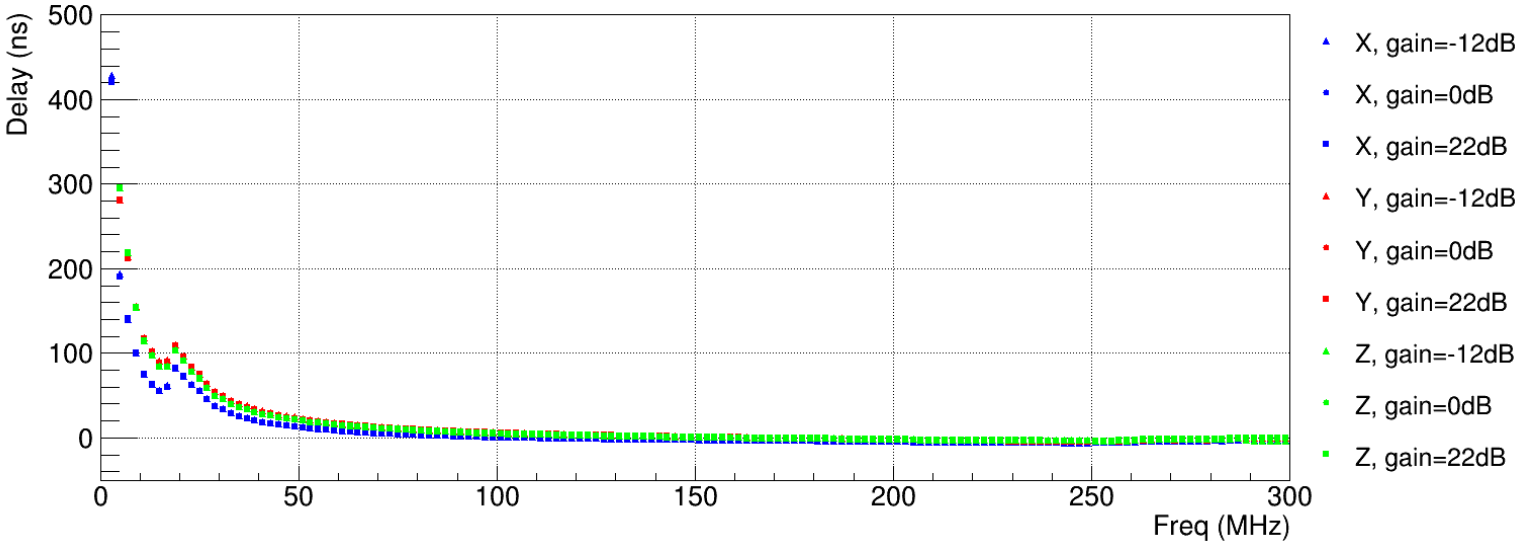

(a) Delay of whole chain

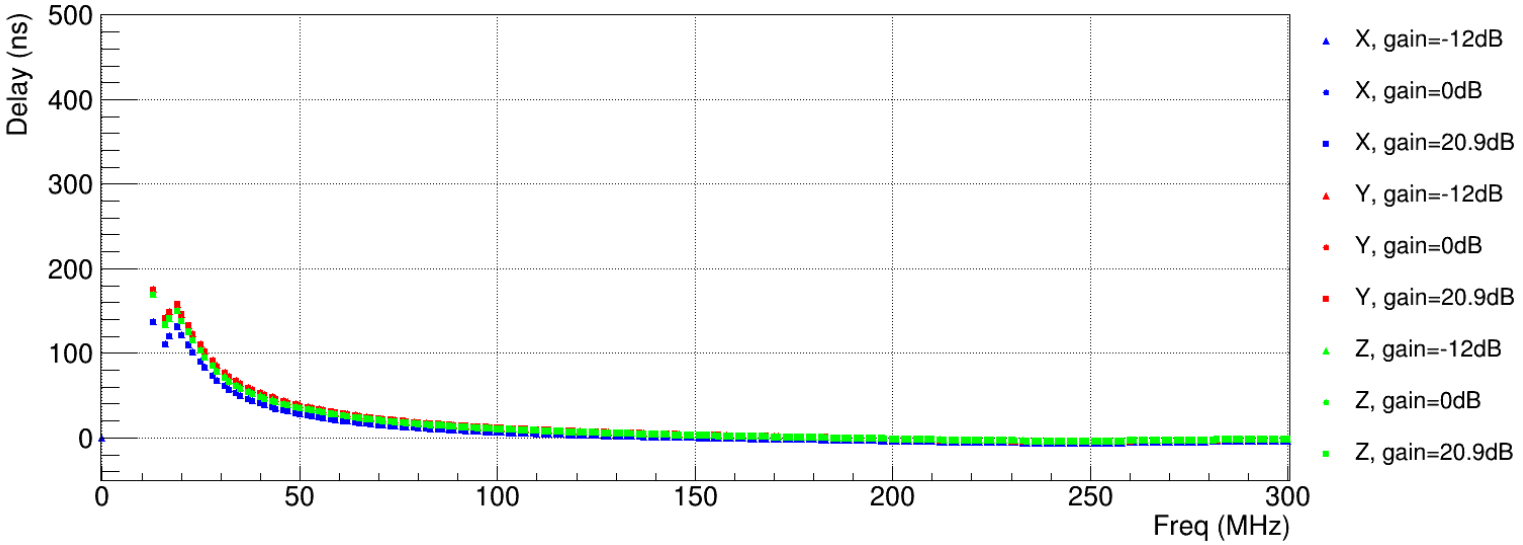

(b) Delay of the separate parts combined afterwards.

Figure B.2

C | Plots of FWHM vs ψ vs θ

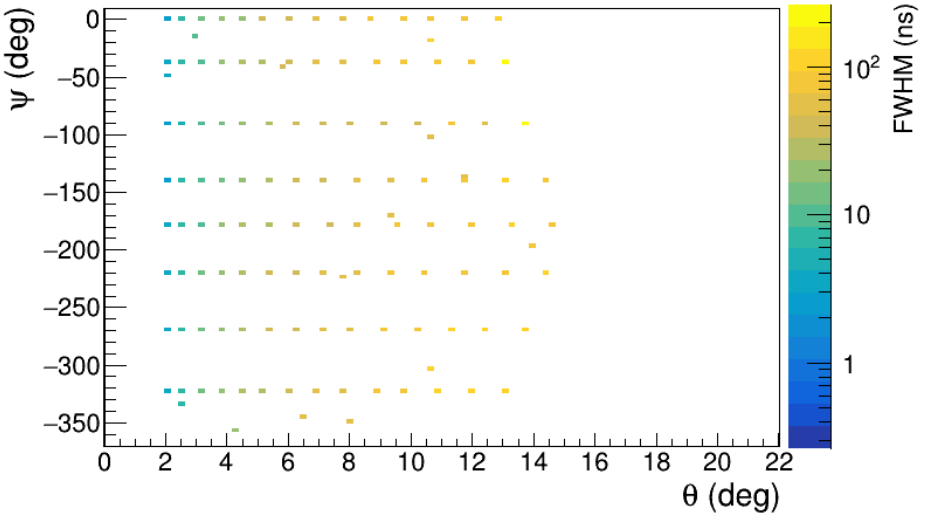

(a) FWHM vs ψ vs θ for a shower with $X_{max} = 711.23$ g/cm^2

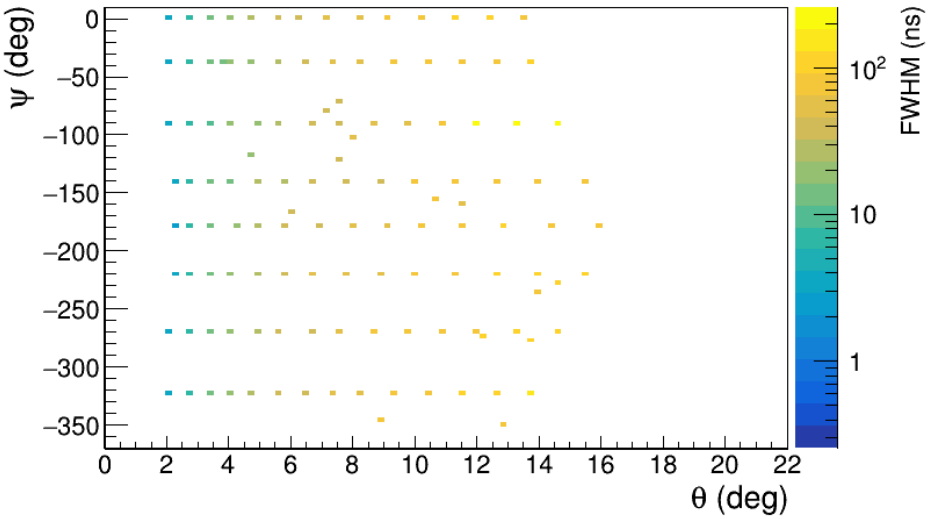

(b) FWHM vs ψ vs θ for a shower with $X_{max} = 737.41$ g/cm^2

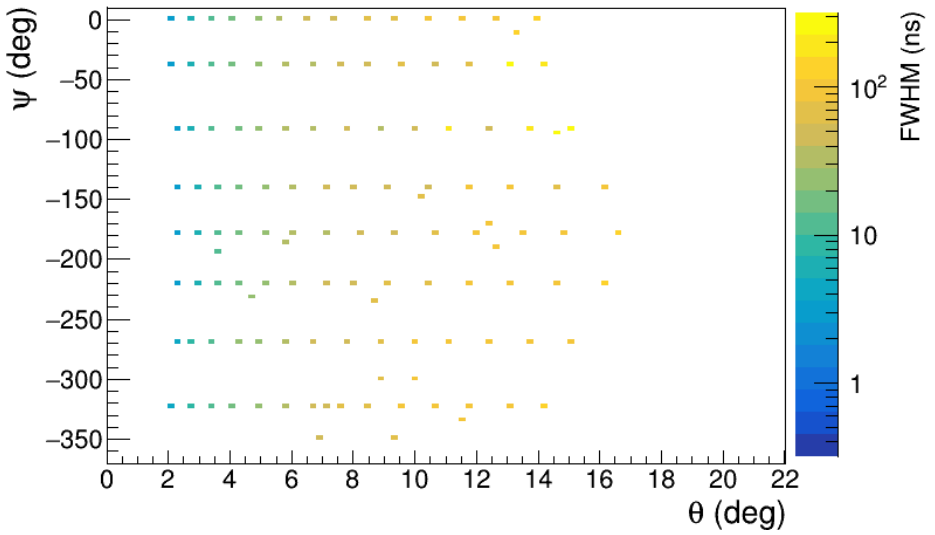

(a) FWHM vs ψ vs θ for a shower with $X_{max} = 756.97$ g/cm^2

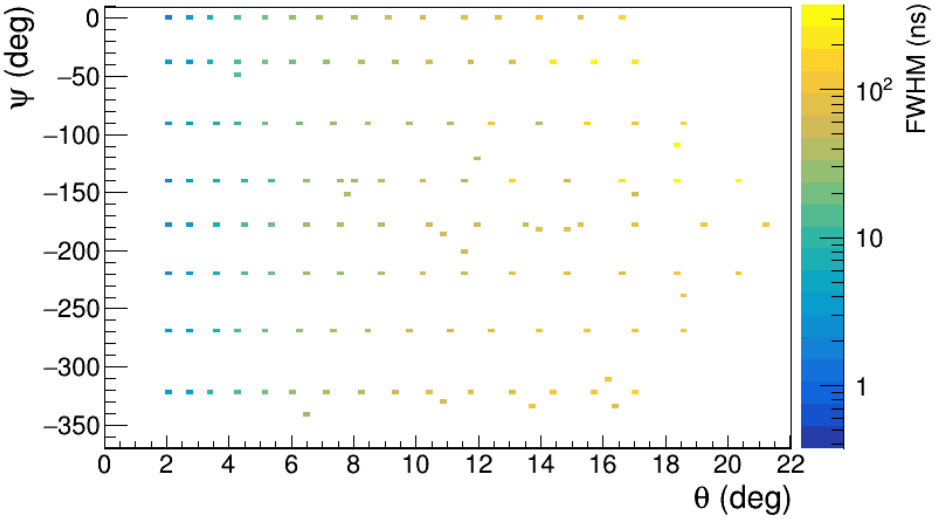

(b) FWHM vs ψ vs θ for a shower with $X_{max} = 853.42$ g/cm^2

D | Plots of FWHM vs θ with the Fits of all Five Depths

Gaussian fit of the peak

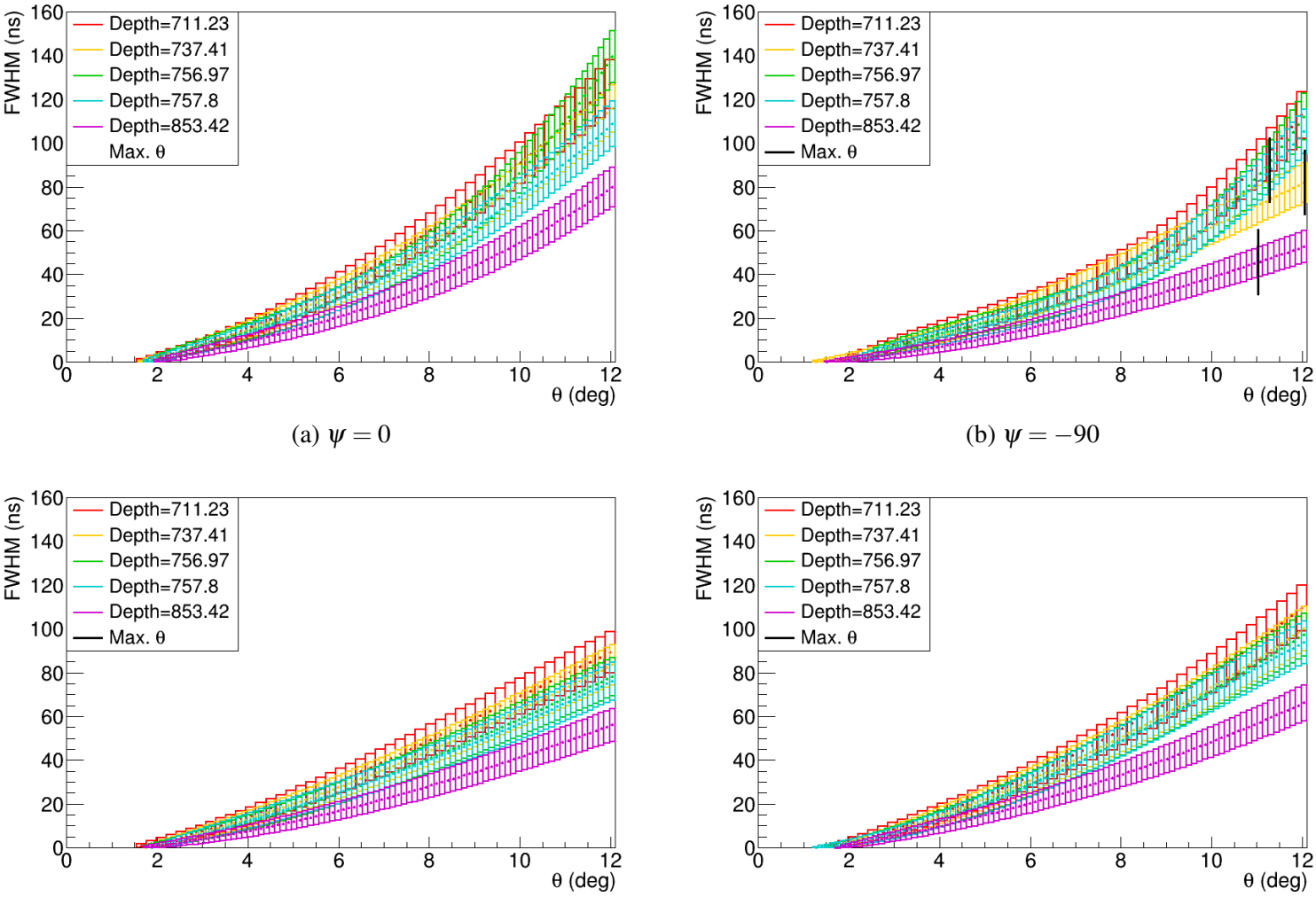

(a) $\psi = 0$

(b) $\psi = -90$

(c) $\psi = -180$

(d) $\psi = -270$

Figure D.1: The fits of the FWHM vs the angle θ with the FWHM from the Gaussian fit of the data.

Landau fit of the peak

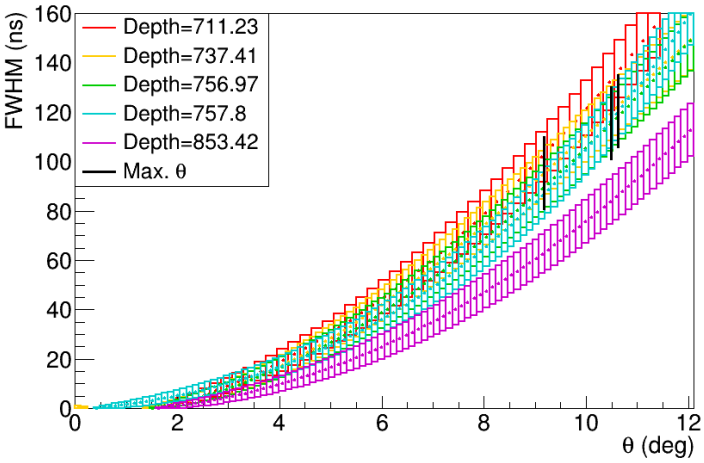

(a) $\psi = 0$

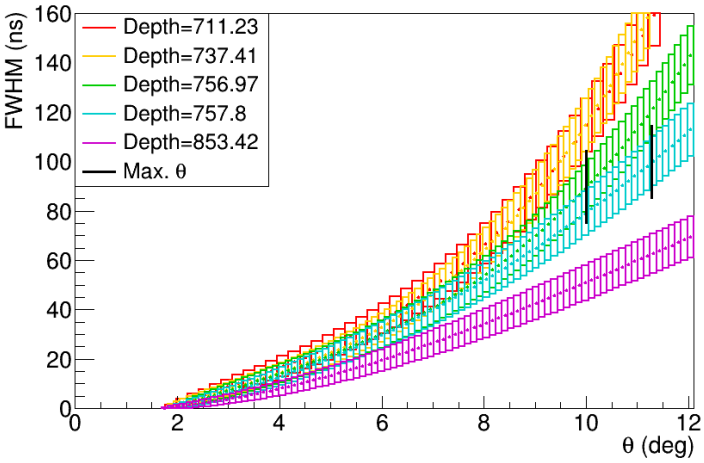

(b) $\psi = -90$

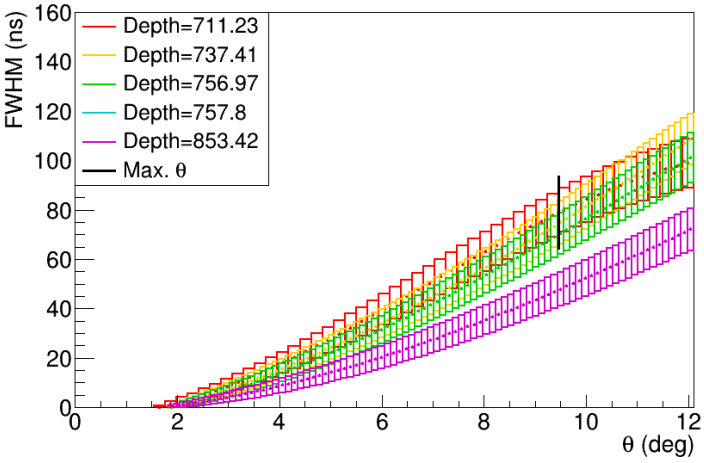

(c) $\psi = -180$

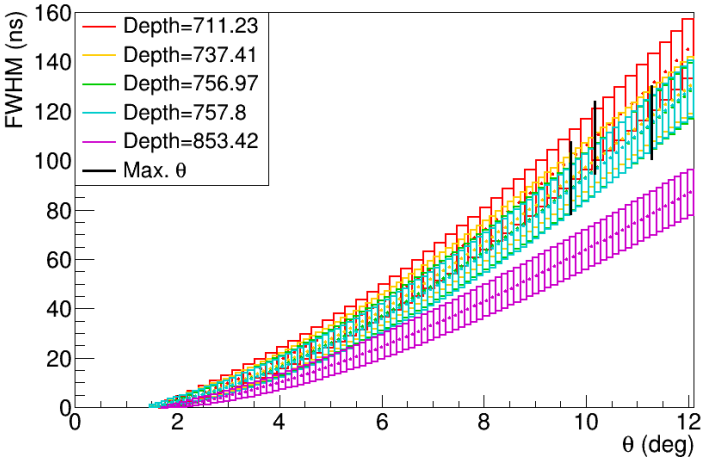

(d) $\psi = -270$

Figure D.2: The fits of the FWHM vs the angle θ with the FWHM from the Landau fit of the data.